JNeurosci
THE JOURNAL OF NEUROSCIENCE

Research Articles: Behavioral/Cognitive

Anterior Thalamic Inputs are Required for Subiculum Spatial Coding, with Associated Consequences for Hippocampal Spatial Memory

https://doi.org/10.1523/JNEUROSCI.2868-20.2021

Cite as: J. Neurosci 2021; 10.1523/JNEUROSCI.2868-20.2021

Received: 12 November 2020
Revised: 24 March 2021
Accepted: 28 March 2021

Title Page

Anterior Thalamic Inputs are Required for Subiculum Spatial Coding, with Associated Consequences for Hippocampal Spatial Memory

Abbreviated Title: Anterior Thalamic Inputs are Required for Subiculum Spatial Coding

Bethany E. Frost[1], Sean K. Martin[1], Matheus Cafalchio[1], Md Nurul Islam[1], John P. Aggleton[2], Shane M. O'Mara[1]*

[1] School of Psychology and Institute of Neuroscience, Trinity College Dublin, Dublin, Ireland; [2]School of Psychology, Cardiff University, Cardiff, United Kingdom

*For correspondence: smomara@tcd.ie

Manuscript Statistics:

Number of figures – 8
Number of tables – 2
Number of words in the Abstract – 125
Number of words in the Introduction – 643
Number of words in the Discussion – 1496

Acknowledgements: This work was supported by a Joint Senior Investigator Award made by The Wellcome Trust to JPA and SMOM (103722/Z14/Z).

Declaration of interests: The authors declare that no competing financial or non-financial interests exist.

Author contributions:

BEF: Acquisition of data, analysis, and interpretation of data, drafting or revising the article

SKM: Developing analysis algorithms, Python script writing and validation, analysis, and interpretation of data, drafting or revising the article

MC: Acquisition of data, analysis, and interpretation of data

MNI: Original conception and development of NeuroChaT

JPA, SMOM: Conception and design, analysis, and interpretation of data, drafting and revising the article

Keywords: Anterior Thalamus, Amnesia, CA1, Hippocampus, Memory, Navigation, Reversible Lesion, Space, Spatial cells, Subiculum

Abstract

Just as hippocampal lesions are principally responsible for 'temporal lobe' amnesia, lesions affecting the anterior thalamic nuclei seem principally responsible for a similar loss of memory, 'diencephalic' amnesia. Compared to the former, the causes of diencephalic amnesia have remained elusive. A potential clue comes from how the two sites are interconnected, as within the hippocampal formation, only the subiculum has direct, reciprocal connections with the anterior thalamic nuclei. We found that both permanent and reversible anterior thalamic nuclei lesions in male rats cause a cessation of subicular spatial signalling, reduce spatial memory performance to chance, but leave hippocampal CA1 place cells largely unaffected. We suggest that a core element of diencephalic amnesia stems from the information loss in hippocampal output regions following anterior thalamic pathology. (125 words)

Significance Statement

At present, we know little about interactions between temporal lobe and diencephalic memory systems. Here, we focussed on the subiculum, as the sole hippocampal formation region directly interconnected with the anterior thalamic nuclei. We combined reversible and permanent lesions of the anterior thalamic nuclei, electrophysiological recordings of the subiculum, and behavioural analyses. Our results were striking and clear: following permanent thalamic lesions, the diverse spatial signals normally found in the subiculum (including place cells, grid cells, and head-direction cells) all disappeared. Anterior thalamic lesions had no discernible impact on hippocampal CA1 place fields. Thus, spatial firing activity within the subiculum requires anterior thalamic function, as does successful spatial memory performance. Our findings provide a key missing part of the much bigger puzzle concerning why anterior thalamic damage is so catastrophic for spatial memory in rodents and episodic memory in humans. (140 words)

Introduction

Bilateral hippocampal formation lesions are the principal cause of the severe and enduring 'temporal lobe amnesic' syndrome (Spiers et al., 2001; Aggleton and Morris, 2018). Bilateral medial diencephalic lesions can also cause a severe and enduring memory syndrome ('diencephalic amnesia'), which can closely resemble temporal lobe amnesia (Kopelman, 1995; Aggleton, 2008). Studies of Korsakoff's syndrome and analyses of thalamic strokes show the anterior thalamic nuclei (ATN: the anteromedial, anteroventral, and anterodorsal nuclei) appear most critical for diencephalic amnesia (Harding, 2000; Van der Werf et al., 2003; Carlesimo et al., 2011; Segobin et al., 2019). Mammillary body damage may also contribute to diencephalic amnesia (Dusoir et al., 1990; Tsivilis et al., 2008), with mnemonic actions via the anterior thalamic nuclei (Aggleton and Brown, 1999; Vann, 2010).

Theories of temporal lobe amnesia assume the hippocampal formation is vital for the brain's cognitive mapping capabilities (Colgin, 2020), and is the core of an extended system vital for human episodic memory (Spiers et al., 2001; O'Mara and Aggleton, 2019). This network model suggests that the anterior thalamic nuclei are key structures within *both* diencephalic and temporal lobe memory systems (Aggleton and Brown, 1999; Ranganath and Ritchey, 2012). In rodents, for instance, anterior thalamic lesions severely impair spatial learning, mirroring hippocampal damage (Morris et al., 1982; Warburton and Aggleton, 1999; Moran and Dalrymple-Alford, 2003); moreover, disconnection studies suggest that the hippocampal formation and anterior thalamic nuclei are functionally-interdependent (Shibata, 1993; Sutherland and Rodriguez, 1989; Nelson et al., 2020).

The hippocampal formation and anterior thalamic nuclei have direct, reciprocal connections via the subiculum (Shibata, 1993), prompting whether anterior thalamic pathology disrupts hippocampal formation functioning, thereby impairing learning and memory. The subiculum also receives indirect ATN inputs via the entorhinal cortices, presubiculum, and retrosplenial cortex. The strategic importance of the subiculum is further evident as it distributes many hippocampal projections beyond the temporal lobe (Meibach and Siegel, 1977; Jay and Witter, 1991; Aggleton, 2012).

Although adjacent, subiculum and hippocampal area CA1 have differing properties. For example, CA1 contains numerous place cells, while the subiculum contains a lower frequency, but greater variety, of spatial cells (place, grid, head-direction, and boundary vector cells) (Thompson and Best, 1989; Brotons-Mas et al., 2010, 2017; Meshulam et al., 2017; Broussard et al., 2020). Furthermore, the anterior thalamic nuclei (especially the anterodorsal nucleus) are a vital source of head-direction information (Taube, 1995; Tsanov et al., 2011); anterodorsal thalamic nucleus lesions eliminate parahippocampal head-direction signals, and disrupt parahippocampal grid cell activity (Winter et al., 2015; Peyrache et al., 2019). Nevertheless, head-direction network disruption does not explain the amnesia associated with anterior thalamic lesions, because lesions of the head-direction system cause only mild, often transient, qualitatively-different, spatial deficits compared to the severe, permanent deficits seen after lesions of anterior thalamic nuclei (Aggleton et al., 1996; Byatt et al., 1996; Dillingham and Vann, 2019).

Given the close anatomical relationship between the subiculum and the anterior thalamic nuclei, we examined how permanent and reversible anterior thalamic nuclei lesions might affect subicular spatial coding and spatial alternation memory. Moreover, hippocampal area CA1 projections to the subiculum show long-term potentiation (O'Mara et al., 2000). We, therefore, made additional recording comparisons with hippocampal area CA1 which, like the subiculum, projects to cortical sites beyond the temporal lobe, but does not receive direct afferents from the anterior thalamic nuclei.

We found that permanent and transient rat anterior thalamic lesions (sparing nucleus reuniens) abrogate spatial signalling by the subiculum. Paradoxically, place coding by CA1 cells remained intact after anterior thalamic lesions, despite spatial alternation dropping to chance levels. The observed silencing seemingly applies to all subicular spatial cell types (place, grid, border, head-direction). Further, because the subiculum is a key source of hippocampal projections beyond the temporal

lobe (Meibach and Siegel, 1977; Irle and Markowitsch, 1982; Jay and Witter, 1991), the impact of anterior thalamic damage as a key component of diencephalic amnesia is amplified. (643 words)

Materials and Methods

Key Resources Table

REAGENT or RESOURCE	SOURCE	IDENTIFIER
Antibodies		
Mouse monoclonal anti-Calbindin	Swant Inc., Switzerland	Cat. #300
Mouse monoclonal anti-NeuN (clone A60)	EMD Millipore, Germany	Cat. #MAB277 Lot #2829834
Mouse monoclonal anti-Parvalbumin	Swant Inc., Switzerland	Cat. #PV235
Rabbit polyclonal anti-Fluorescent Gold	EMD Millipore, Germany	Cat. #AB153-1 Lot #2905401
Biotinylated horse anti-rabbit IgG (H+L)	Vector Laboratories, UK	Cat. #BA-1100
Biotinylated horse anti-mouse IgG (H+L)	Vector Laboratories, UK	Cat. #BP-2000
Critical Commercial Assays		
DAB Peroxidase (HRP) Substrate Kit (with Nickel), 3,3'-diaminobenzidine	Vector Laboratories, UK	Cat. #SK4100
Vectastain Elite ABC HRP Kit (Peroxidase, Standard)	Vector Laboratories, UK	Cat. #PK6100
Deposited Data		

Raw and analyzed data	This paper	https://osf.io/vdakx/
Experimental Models: Organisms/Strains		
Rat: Lister Hooded (male)	HsdOla:LH	Envigo, UK
Software and Algorithms		
FIJI (**F**iji **I**s **J**ust **I**mageJ)	Schneider et al., 2012	https://imagej.net/Fiji
TINT	Axona Ltd, UK	http://axona.com/
R Statistics	R Core Team, 2017	https://www.r-project.org/
NeuroChaT	Islam et al., 2019	https://github.com/shanemomara/omaraneurolab
Other		
25µm platinum-iridium wire	California Fine Wire, USA	Cat. #100167

Lead Contact and Materials Availability

Requests for further information and resources should be directed to and will be fulfilled by the Lead Contact, Shane O'Mara (smomara@tcd.ie). This study did not generate new unique reagents.

Subject Details

Experiments were conducted on 23 male Lister Hooded rats (Envigo, UK) with pre-procedural weights of 309-356 g. Upon arrival, animals were cohoused on a 12-hour day/night cycle and handled daily by the experimenter for a week before surgical procedure. Prior to surgery and during recovery, animals had free access to food and water; during behavioural testing, food was restricted,

but ensured the animals did not fall below 85% of the animal's free feeding weight. All rats were naïve prior to the present study. Selection of animals between lesion and control groups was alternated according to body weight prior to surgery (starting with the heaviest), so that pre-procedural weights were matched, and the groups balanced.

Experimental Design

During stereotaxic surgery, rats were implanted unilaterally with twenty-eight electrodes of 25 µm thickness platinum-iridium wires (California Fine Wire, USA) arranged in a tetrode formation. Tetrodes were targeted at the dorsal subiculum, CA1, or at the subiculum and CA1 simultaneously. An additional bipolar electrode (stainless steel, 70 µm thickness) targeting the ipsilateral retrosplenial cortex (RSP) was also implanted in all but two cases (see below), but the data from these electrodes are considered elsewhere. All electrodes were connected to a 32-channel microdrive (Axona Ltd., UK).

For the permanent lesion experiments, seven animals received stereotaxic cytotoxic lesions targeting the anterior thalamic nuclei ('ATNx'), followed by electrode implantation targeting dorsal subiculum and RSP. Meanwhile, three rats underwent sham injections of equivalent volumes of PBS only ('Sham' controls). A further four rats ('Normal' controls) had no sham lesion procedure, i.e., just had electrodes implanted. Both the sham and normal controls had electrodes targeting dorsal subiculum.

The temporary inactivation (muscimol) experiment followed the permanent lesion study. For this, a further six animals (ATNmusc) were implanted with tetrode and bipolar electrode configurations alongside bilateral infusion cannulae (26 gauge, 4 mm length, Bilaney Consultants Ltd., UK) in the ATN. Electrodes were positioned as above, with two exceptions; one animal was implanted with four tetrodes targeting the subiculum, three targeting CA1 and one targeting retrosplenial cortex, with no additional bipolar electrode; and one rat was implanted with tetrodes targeting the subiculum and the bipolar electrode targeting CA1.

Finally, for the CA1 experiment, a further three rats (ATNx_CA1) received permanent bilateral cytotoxic ATN lesions followed by electrode implantation into CA1.

Ethics

All experimental procedures were in accordance with the ethical, welfare, legal and other requirements of the Healthy Products Regulatory Authority regulations, and were compliant with the Health Products Regulatory Authority (Irish Medicines Board Acts, 1995 and 2006) and European Union directives on Animal Experimentation (86/609/EEC and Part 8 of the EU Regulations 2012, SI 543). All experimental procedures were approved by the Comparative Medicine/Bioresources Ethics Committee, Trinity College Dublin, Ireland prior to conduct, and were carried out in accordance with LAST Ireland and international guidelines of good practice.

Surgical methods - permanent ATN lesions and electrode placements

Rats were first anesthetised with isoflurane (5% to induce anaesthesia, 1-2% to maintain) combined with oxygen (2 L/minute). After being placed in a stereotaxic frame, chloramphenicol 0.5% eye gel, pre-operative antibiotics (Enrocare, 0.1 ml in 0.5 ml saline) and analgesia (Metacam, 0.1 ml) were administered.

The skull was exposed, and connective tissue removed. For the ATNx cohort (n = 7), bilateral neurotoxic lesions targeting the ATN were performed using slow infusions of 0.12 M *N*-methyl-D-aspartic acid (NMDA) dissolved in phosphate buffer solution (PBS, pH 7.35). NMDA was infused over 5 minutes (0.22 or 0.24 µl per site) via a 0.5 µl Hamilton syringe (25 gauge), with the syringe left in position a further 5 minutes at each of four target sites before slow retraction. The craniotomies were then sealed using bone wax (SMI, St Vith, Belgium). The ATN lesion coordinates, with the skull flat, were as follows from bregma: AP -1.7 mm, ML ±0.8 mm, DV -5.7 mm from top of cortex; AP -1.7 mm, ML ±1.6 mm, DV -4.9 mm from top of cortex. Sham control animals (n = 3 rats) underwent four equivalent infusions of PBS only.

Bundles of 28 electrodes of 25 µm thickness platinum-iridium wires (California Fine Wire, USA) arranged in a tetrode formation were implanted unilaterally. Tetrodes were implanted aimed at the dorsal subiculum (AP -5.6 mm, ML 2.5 mm, DV -2.7 mm from top of cortex), CA1 (AP -3.8 mm, ML 2.5 mm, DV -1.40 mm from top of cortex), or both. Electrodes were stabilised with dental cement (Simplex Rapid, Kemdent, UK) attached to the screws implanted into the skull. An additional bipolar electrode (stainless steel, 70 µm thickness) targeting the ipsilateral retrosplenial cortex (RSP) was also implanted in all but two cases, the data from which are considered elsewhere. All electrodes were connected to a 32-channel microdrive (Axona Ltd., UK).

For the ATN inactivation experiment, a further six animals (ATNmusc) were implanted with tetrode and bipolar electrode configurations alongside bilateral infusion cannulae (26 gauge, 4 mm length, Bilaney Consultants Ltd., UK). Cannulae were placed targeting ATN (AP -1.7 mm, ML ±3.8 mm, DV -4.0 mm from top of cortex, at angle 28.6° towards centre), then fixed in position using dental cement and dummy cannulae inserted to prevent blockage. Electrodes were positioned as above, targeting dorsal subiculum and RSC, with two exceptions; one animal was implanted with four tetrodes targeting the subiculum, three targeting CA1 and one targeting retrosplenial cortex, with no additional bipolar electrode; and one rat was implanted with tetrodes targeting the subiculum and the bipolar electrode targeting CA1.

Glucosaline (5-10 ml) was administered subcutaneously post-operatively and the animal allowed to recover. Animal weight, activity, and hydration were closely monitored daily for a minimum of 7 days before beginning electrophysiological recordings.

Electrophysiological recordings

Electrophysiological recordings were obtained using an Axona Ltd (UK) 64-channel system, allowing dual recordings of single units and local field potentials (LFP) from each electrode. Initial habituation recordings were conducted in a 60 x 60 cm square, walled arena (height 42 cm). Later testing involved a larger arena (105 x 105 cm, 25 cm height). For both arenas, the walls and floors were

made of wood painted matt black. A black curtain could be closed around the arena to remove distal spatial cues, and visual cues could be attached to the curtain as required. The habituation sessions in the small arena allowed the animal to acclimatise to the recording procedure and the experimenter to adjust electrode locations until the optimal recording depth was reached. After the habituation period (usually 3-7 days), rats were first trained on the behavioral tasks (T-maze then bow-tie maze) with up to one hour of free exploration with pellet-chasing tasks typically recorded afterwards in the same day. Pellet-chasing included the rotation of spatial cues on the curtain during the recording of single unit activity in the small arena to examine whether spatial units remap accordingly, exploration in the small then large arena in order to assess spatial cell remapping, and consecutive recordings to examine sleep properties (data not described here).

Behavioral tasks

Spatial alternation

A four-arm cross-shaped wooden maze with raised sides (119 x 119 cm full length; each arm 48 x 23 cm; height 30 cm) was used for the spatial alternation task, allowing the rotation of start points. Each arm could be blocked close to the centre to form a T-maze. In addition, a barrier could be placed within an arm to form a holding area for the start position. Distal spatial cues were available in the recording room including the pulled-back curtain, electrophysiological recording equipment set on wall-mounted shelves, a desk and computer. Animals were first habituated in pairs to the maze and allowed to freely explore for 10 minutes. Rats then individually had two pre-training sessions (5 minutes each) in which they were first placed behind a barrier at the start position at one end of the maze, retained for 10 seconds, then the door removed and the rat allowed to explore the maze. The maze arm opposite to the start was blocked and sucrose pellets (TestDiet 5TUL 20mg, USA) were placed in a shallow dish at the end of each open arm so that they were not visible from the centre of the maze. Rats learnt to run to an arm of the maze to obtain sucrose pellets, which were replaced once they had been consumed and the animal left that arm. The maze was then

185 altered so that a different start arm and blocked arm were used, and another training session run.
186 Each rat had four 5-minute training sessions per day such that each start/blocked configuration was
187 experienced (opposite, adjacent, opposite) for two days initially, with an additional day if required.

188 For the experiment, rats were placed in the start position for 10 seconds. In each trial, there was an
189 initial forced run ('sample'), in which two arms of the cross-shaped maze were blocked forcing the
190 animal into either the left or right arm in order to obtain two sucrose pellets from the end of the
191 arm. The animal was then picked up and returned to the start position and held for approximately
192 20 seconds before being released for the choice run ('test'), in which one of the barriers was
193 removed from the maze so that the animal had the choice of either the left or right arm (Fig. 2A).
194 Sucrose pellets were only available in the arm opposite to the sample run, so the rat was rewarded if
195 it alternated. A choice was determined when the back paws of a rat had entered the arm. The rat
196 was then removed from the maze and placed in an open holding cage for 2-3 minutes whilst the
197 maze was rearranged. Each animal had eight sessions consisting of eight trials each, with both the
198 start position and forced turn pseudorandomised so that the same arrangement did not occur more
199 than twice consecutively. Rats were connected to the electrophysiological recording equipment
200 throughout pre-training and each test session.

201 *Bow-tie maze*

202 The bow-tie maze allows continuous object recognition testing, with multiple trials and new novel
203 objects during each session (Albasser et al., 2010). The bow-tie shaped maze had raised sides (wood
204 painted matt black; 120 cm long x 50 cm wide, 50 cm height) and a central sliding. Partitions at each
205 end of the maze split both ends into two short corridors (Fig. 2C). The animals were first habituated
206 to the maze for 10 minutes, by allowing free exploration with sucrose pellets scattered throughout.
207 Next, during the 10 minute session, pellets were first placed in wells at the two ends of the maze and
208 the rat trained to run from one end of the maze to the other when the central door was opened.
209 Then, opaque plastic objects (a funnel and a beaker) were placed behind each baited well. The

objects were gradually moved so that they increasingly covering the wells. Rats underwent 4-5 ten minute pre-training sessions, until they readily shuttled across the maze to retrieve sucrose pellets by pushing objects.

For the experimental procedure, 22 pairs of novel objects were used. In the first trial, one novel object was placed covering the sucrose pellets. The rat retrieved the pellets and investigated the object at that end of the maze. After 1 minute, the central door was opened and the rat passed to the opposite end of the maze, where there would be a repeat of the original object (now familiar) and a new novel object (both covering sucrose pellets). This procedure was repeated for all 22 pairs of objects, so that each of the 21 trials consisted of a new novel object and the previous object, which was now familiar (Albasser et al., 2010). Animals were video recorded throughout.

For analysis, the time spent investigating each object was recorded and two measures of recognition, D1 and D2, were calculated (Albasser et al., 2010). D1 represents the difference in exploration time between novel and familiar objects, and is calculated by subtracting the time spent exploring a familiar object from the time spent exploring a novel object. Cumulative D1 represents the sum of the exploration time for all novel objects minus the sum of exploration time for all familiar objects across all trials. D2 represents the total difference in exploration time (cumulative D1) divided by the total exploration time for both novel and familiar objects, resulting in a ratio that ranges between +/- 1.

Transient inactivation of the ATN (muscimol)

An additional cohort (n = 6, ATNmusc) was implanted with bilateral infusion guide cannulae (26 gauge, 4 mm length; Bilaney Consultants Ltd., UK) aimed at the ATN at an angle of 28.6° towards the midline (AP -1.7 mm, ML ±3.6 mm, DV -4.0 mm from top of cortex) alongside subiculum electrode implantation. A dummy cannula (0.203 mm diameter, 4 mm length; Bilaney Consultants Ltd., UK) was used to protect each guide cannula during recovery and normal recording activity. All other

surgical and electrophysiological methods were the same as those used for the animals with permanent ATN lesions.

Following recovery, rats were trained daily for a minimum of one week prior to commencing inactivation experiments. Rats were lightly restrained and the dummy cannulae removed and replaced several times. During this period, rats were also trained in the spatial alternation (T-maze) task and electrophysiological activity was recorded during free exploration and pellet-chasing in the large and small square arenas. All apparatus matched that used for the ATNx rats.

On the day of experimentation, electrophysiological recordings of exploration and pellet-chasing were first performed pre-infusion for 20-40 minutes to establish a baseline. The animal was then lightly restrained and muscimol (concentration 0.5 mg / 1 ml saline) infused through a 33 gauge infusion needle with a 1- or 2 mm projection past the length of the implanted guide cannula, targeting the ATN. Muscimol was infused over 90 seconds using a 0.5 µl Hamilton syringe and infusion pump (KD Scientific, Hollister, USA). The infusion needle was retained in position for a further 60 seconds before it was removed and replaced with the dummy cannula. Rats received a 0.2 µl at each of two locations per hemisphere using both a 5- and 6 mm length infusion needle to target the whole ATN (Fig. 1H). Following infusion, electrophysiological recordings during pellet-chasing and exploration were conducted in consecutive 20 minute sessions in the small and large square arena. Arenas were swapped between recordings to maintain the animal's interest in the surroundings and to assess whether spatial remapping occurred. Between 90 and 120 minutes into the experiment, the T-maze task was performed (8 trials, pseudo-randomised starting points). Animals were then returned to the square arena and recorded for a further 2-3 hours, including during sleep. Regular diet and water were freely available in the recording arena after the T maze test. The following day, further electrophysiological recordings were undertaken to determine whether the effects of muscimol had ceased and cell activity had returned to baseline.

Muscimol infusions were repeated 1-2 weeks after the initial experiment. In two cases, an additional control infusion of saline was given. To visualise the location of the muscimol infusion, the tracer fluorogold (Sigma-Aldrich Ireland Ltd, Ireland) was infused one day prior to perfusion.

Perfusion and histology

After completion of experiments, animals were sacrificed and perfused transcardially with 0.1 M phosphate buffered saline (PBS) then 2.5% paraformaldehyde (PFA) in 0.1 M PBS. Brains were removed and post-fixed in PFA for 24 hours then transferred to 30% sucrose in 0.1 M PBS solution for 2 days. A cryostat (Leica CM1850) was used to cut 40 µm sections in a 1:4 series. One series was mounted onto double gelatin-subbed microscope slides and, once completely dry, washed in decreasing concentration of alcohol (100, 90, 70%) before being stained with cresyl violet, a Nissl stain (Sigma-Aldrich Ireland Ltd, Ireland). Sections were then dehydrated with increasing alcohol concentrations, washed in xylene, and cover-slipped.

Of the other series, one was reacted against anti-calbindin antibody raised in mouse (Swant Inc., Marly, Switzerland) and another against anti-NeuN antibody raised in mouse (EMD Millipore, Germany). The remaining series was reacted with either anti-parvalbumin antibody raised in mouse (Swant Inc., Marly, Switzerland) or, in the temporary inactivation cohort, with anti-fluorogold raised in rabbit (EMD Millipore, Germany).

In brief, sections were washed in a quench solution (10% methanol and 0.3% hydrogen peroxide in distilled water) before PBS (0.1 M pH 7.35) then PBST (2 ml Triton X-1000 in 1 litre 0.1 M PBS; pH 7.35) washes. Sections were stirred for one hour in 4% normal horse serum in PBST before the primary antibody was added (1:5000 dilution in PBST for calbindin, parvalbumin and fluorogold; 1:10000 for NeuN) and stirred at 4° overnight. Sections were then washed in PBST before being incubated for two hours in 1:250 dilution of horse-anti-mouse (Vector Laboratories, UK), or, in the case for fluorogold, horse-anti-rabbit (Vector, UK), in PBST. After further PBST washes sections were incubated at room temperature in Vectastain Elite ABC Solution (Vector Labs, UK) before further

PBST and PBS washes. Sections were then reacted with DAB solution (Vector Labs, UK) and washed in PBS.

All sections were mounted on double-subbed slides, and fluorogold reacted slides were lightly stained with cresyl violet for improved tissue visualisation before cover-slipping. Sections were imaged using either an Olympus BX51 upright microscope or Leica Aperio AT2 slidescanner.

Statistical Analyses

Behavioral analysis

To analyse T-maze results, the mean score was compared between Normal Control, Sham Control and ATNx groups using ANOVA with Tukey *post hoc* test. For the muscimol experiments, T-maze results during ATN inactivation were compared to the same animals before inactivation.

To analyse object recognition using the bow-tie maze, the time spent investigating each object was recorded and two measures of recognition, D1 and D2, were calculated (Albasser et al., 2010).

Unit identification and isolation

Spike sorting was performed automatically in Tint using k-means (Axona Ltd., Herts, UK) and cluster cutting refined manually. Unit identification used the following criteria: units had to be active, and show consistent waveform characteristics (amplitude, height, and duration) during recording, as well as a clean refractory period (>2 ms) in the inter-spike interval (ISI) histogram. Spike amplitude was measured as the difference between the positive peak and the first negative peak before the positive peak, if present, or zero. Spike height was the difference between the spike peak to the minimum value of the spike waveform. Spike width was the distance in microseconds beyond which the waveform drops below 25% of its peak value. Histograms were used to assess spike width and determine whether qualitatively different neuron populations were being recorded following anterior thalamic lesions.

306 Units were sometimes seemingly recorded for more than 1 day, despite electrode lowering. For
307 these cases, cells were monitored on the relevant tetrodes from day-to-day; for analysis, only clean
308 recordings with the largest sample size and spikes of the highest amplitude were chosen. To avoid
309 double-counting cells, care was taken to exclude seemingly-related samples from analysis. During
310 spike sorting, the signals from each cell were carefully followed from first appearance to complete
311 loss, to avoid overestimation of cell counts. Once well-defined neuronal signals were isolated
312 recording commenced. For permanent lesion experiments, rats had to explore at least 90% of the
313 arena in a session to be included in analyses to allow reliable calculation of spatial characteristics.

314 Standard statistical testing was performed using an open-source custom-written suite in Python
315 (NeuroChaT (Islam et al., 2019); available for download at
316 https://github.com/shanemomara/omaraneurolab), and additional custom codes in R (R Foundation
317 for Statistical computing, Vienna, Austria, https://www.r-project.org). Units were classified based on
318 the spatiotemporal features of their activity in the arena during pellet-chasing, as described below.

319 **Bayesian analysis**

320 To investigate whether the apparent absence of spatial signal in ATNx animals was significant, a
321 Bayesian approach was applied as follows. Let PC denote the probability that a control recording will
322 contain a spatial cell, and PL denote the probability that a lesion recording will contain a spatial cell.
323 Let D denote the recorded data. By Bayes theorem, $P(PC, PL \mid D) = P(D \mid PC, PL) * P(PC, PL) / P(D)$
324 (i.e. posterior = likelihood * prior / probability of the evidence). We use a uniform prior distribution,
325 as we have no prior belief of how common recordings in the subiculum with spatial cells are, so
326 $P(PC, PL) = 1$. The probability of the evidence is a constant normalising parameter, which can be
327 calculated by ensuring the posterior distribution sums to 1. By the independence assumption of
328 selected recordings, the likelihood function can be modelled as the product of evaluating the
329 probability mass functions arising from two binomial distributions:

$$P(D \mid PC, PL) = \binom{CR}{CS} PC^{CS}(1-PC)^{CR-CS} \binom{LR}{LS} PL^{LS}(1-PL)^{LR-LS}$$

Where the data D, provides the information; CR: the number of control recordings, CS: the number of control recordings with a spatial cell, LR: the number of lesion recordings, and LS: the number of control recordings with a spatial cell. As an example, using the data from the contingency table for the recordings with spatial cells (Table 1):

$$P(D \mid PC, PL) = \binom{53}{15} PC^{15}(1-PC)^{53-15} \binom{47}{0} PL^{0}(1-PL)^{47-0}$$

Burst properties

Bursting units were identified using criteria based on Anderson and O'Mara (Anderson and O'Mara, 2003). A burst was defined as a series of spikes in which each inter-spike interval (ISI) was a minimum of 6 ms, and contained a minimum of two spikes, with a minimum inter-burst interval (IBI) of 50 ms. Further bursting analyses examined the total number of bursts during a recording session; the number of spikes in the bursting cluster; mean inter-spike interval during the burst cluster; number of spikes per burst; burst duration; duty cycle (the portion of an inter-burst interval during which a burst fires); the inter-burst interval; and propensity to burst, calculated by dividing the number of bursting spikes by the total number of spikes in a recording.

Spatial analyses

Additional analyses examined spatial modulation of recorded units. Multiple indices were used to analyse the spatial properties of unit activity (namely spatial coherence, spatial information content, and spatial sparsity). A firing field was defined as a set of at least nine contiguous pixels with firing rate above zero. A place field was identified if nine neighbouring pixels (sharing a side) were above 20% of the peak firing rate. Place field size was represented by number of pixels. Spatial specificity (spatial information content) was expressed in bits per spike (Skaggs et al., 1996). Mean spiking frequency is the total number of spikes divided by the total recording time and is expressed in

spikes/s. Exploration was assessed by comparing the occupancy of bins and the number of visits per bin during recording sessions. Additionally, to be regarded as place cells, the following criteria had to be met: all included as place cells had to have a spatial information content (Skaggs et al., 1996) index of > 0.5; a spatial coherence of > 0.25; and a mean firing rate > 0.25. The spatial path of the subject and the spike train were used to produce a locational firing rate map.

To analyse head direction (HD) cells, the animal's head direction was calculated using the relative position of two tracked LEDs on a bar attached to the microdrive, in the horizontal plane. The directional tuning function was determined by plotting the firing rate as a function of the HD divided into 5° bins, and the firing rate calculated by the total number of spikes divided by time spent in each bin.

To determine the existence of a hexagonal grid firing structure, grid index, size and orientation were calculated. The grid cell analysis included calculating the spatial autocorrelation of the firing rate map and assessing the shape formed by the peaks in autocorrelation. For border cell analyses, cells with a firing profile that was parallel to the border of the arena were selected by plotting the positional firing pattern.

Down-sampling analysis

We performed a spatial down-sampling procedure as a control method to rule out the possibility that the disruption in spatial firing merely reflects a lack of sampling of the environment, given that the animals move less distance and cover less of the environment while under the effects of muscimol.

Our method is based on the spatial down-sampling performed by Boccara et al. (Boccara et al., 2019): for each cell, we produce a list *L = (x_t, y_t, spike_t)* where *x_t, y_t* is the position of the animal at time *t* and spike_t is the number of spikes the cell emitted in that time bin. The procedure to spatially down-sample data from recording A to match the exploration in recording B is as follows.

Firstly, the list L from B is binned into 3cm squares based on x_t, y_t and the list L from A is binned using the same number of bins as was used for B. Secondly, several random samples are drawn (with repetition) from the list L in A such that the number of samples drawn from an individual bin is the minimum of the number of data points falling in that bin between recordings A and B. Using this spatially down-sampled data, firing rate maps and spatial statistics are performed as in the rest of this paper. This procedure is performed 200 times for each cell.

Using the method above, recordings were spatially down-sampled to match their own spatial occupancy as an additional control since the random sampling procedure should cause small changes. After testing spatial coherence, spatial information content, and spatial sparsity, coherence was the only measure tested which was resistant to down-sampling against self (mean decrease of 0.015) and down-sampling to other random data (mean decrease of 0.05).

For each cell considered in the muscimol experiments, the baseline recording was down-sampled to match the muscimol recordings, and the muscimol recordings were down-sampled to match the baseline recording. These resulting firing maps had closely matching occupancy of the environment, and coherence was computed on these maps.

Image analysis

Individual images of sections were aligned and tiled using Inkscape (http://inkscape.org) and FIJI (**F**iji **I**s **J**ust **I**mage J, https://imagej.net/Fiji (Preibisch et al., 2009)). Cresyl violet stained sections helped to confirm electrode placement. To assess lesion success, the ATN was segmented from photomicrographs of anti-NeuN reacted sections using FIJI and the resulting image thresholded to show nuclei separation, before using the inbuilt Analyse Particles plugin to obtain a cell count. The ATN cell counts were compared between the ATNx and control groups to determine lesion effectiveness. Calbindin-reacted sections helped to determine the status of nucleus reuniens.

Statistical analysis

Statistical analyses were performed in R Statistics (https://www.r-project.org/). No statistical difference was noted between Normal Control and Sham Control groups, so these were combined into a single Control group unless otherwise stated. Distribution of variables was assessed using histograms, and where a normal distribution was determined, differences between groups were examined using Welch's Two-Sample *t*-test, an adaptation of Student's *t*-test that is more reliable when samples have unequal variances or sample sizes. Where three groups were compared, ANOVA with a Tukey *post-hoc* test was applied. In cases where the distribution of a variable was non-parametric, differences between groups were assessed using Mann-Whitney U test.

For temporary inactivation experiments, data were compared to baseline (immediately prior to muscimol infusion) values using Welch's Two-Sample *t*-test with a Bonferroni correction to account for multiple comparisons and reduce the likelihood of Type 1 errors.

Statistical tests are reported in the text and appropriate figure legends, (* $p < 0.05$, ** $p < 0.01$, *** $p < 0.001$). Boxplots show median, 25^{th} and 75^{th} percentiles. Boxplot tails represent the smallest and largest value within 1.5 times the interquartile range, and outliers are defined as values that are > 1.5 times and < 3 times the interquartile range. Data means are represented with a diamond-shaped marker. Error bars on scatter plots represent standard error of the mean (SEM).

Data and Code Accessibility

Datasets generated during this study are available at OSF (https://osf.io/vdakx/) and code is available at GitHub (https://github.com/shanemomara/omaraneurolab). Further information will be available upon request by contacting Shane O'Mara (smomara@tcd.ie).

Results

Throughout, the terms hippocampal formation and hippocampal refer to the dentate gyrus, the CA fields, and the subiculum. The parahippocampal region includes the presubiculum, parasubiculum, postsubiculum and entorhinal cortices. Recordings of neuronal activity were conducted in the subiculum and area CA1. Spatial alternation memory and object recognition memory were assessed using a T-maze and a bow-tie shaped maze, respectively. Rats received permanent neurotoxic lesions of the anterior thalamic nuclei (ATNx) following injections of *N*-methyl-D-aspartic acid (NMDA), or transient ATN lesions following infusion of muscimol. Other rats served as controls.

Combining anterior thalamic nuclei lesions (NMDA) with implantations in the dorsal subiculum

Of 23 animals implanted, one ATNx rat was subsequently excluded due to electrode malfunction, and one normal control was excluded because of post-surgical complications. Comparisons between the normal control and sham control groups consistently failed to reveal group differences and, for this reason, they were typically combined (group 'Control').

N-methyl-D-aspartic acid injections caused considerable cell loss within the anterior thalamic nuclei, but spared nucleus reuniens

Lesion effectiveness was quantified by comparing the total anti-NeuN reacted cell counts in 40µm thick brain sections containing the anteromedial, anterodorsal, and anteroventral thalamic nuclei in ATNx animals with the corresponding Control values (Fig. 1A, B). The ATNx rats had markedly reduced cell counts (Control 16209 ± 2507, ATNx 3497 ± 1528; $t_{(8.26)} = -9.68$, $p < 0.001$, Welch's Two Sample *t*-test; Fig. 1E), while the calbindin-reacted sections helped to confirm that nucleus reuniens remained intact (Fig. 1C, D), indicating that, despite a significant role in spatial working memory (Griffin, 2015), nucleus reuniens damage was not a contributing factor to differences in either behaviour or cell firing properties in ATNx animals.

ATN lesions (NMDA) reduce spatial alternation memory to chance levels of performance

444 Unless otherwise stated, Welch's Two Sample *t*-tests were performed to compare Control and lesion
445 data.

446 Consistent with previous lesion studies, ATNx animals had considerably lower spatial alternation
447 scores (52.23 ± 14.58%), compared to Normal (83.10 ± 10.96%) and Sham (81.25 ± 11.41%) controls
448 (ANOVA, $F_{(2,\ 114)}$ = 77.8, p < 0.001; Tukey post-hoc p < 0.001; Fig. 2B), confirming their severely
449 impaired spatial working memory. In contrast, ATNx animals showed no impairment in novel object
450 discrimination when compared to the Control animals (cumulative D1 $t_{(142.69)}$ = 0.99, p = 0.324;
451 updated D2 $t_{(172.25)}$ = 1.42, p = 0.159) indicating that recognition memory under these conditions
452 remains intact (Fig. 2D-F). During free exploration in the square arenas with electrophysiological
453 recordings, the ATNx rats travelled greater distances than the Control animals both during
454 habituation (Control l 62.14 ± 17.43 m, ATNx 85.45 ± 14.21 m; $t_{(16.14)}$ = 3.55, p = 0.003) and during
455 subsequent recordings (Control 120.66 ± 15.19 m, ATNx 142.41 ± 10.89 m; $t_{(14.55)}$ = 2.98, p = 0.096),
456 suggesting slightly increased motor activity post-ATNx.

457 **ATN lesions (NMDA) abrogate spatial firing in the subiculum only: Quantitative analyses**

458 Spatial and non-spatial single units were recorded in the dorsal subiculum of all animals. Of 82 single
459 units recorded in the Control rats, 47 (57%) were considered spatial units (Fig. 3A). These units
460 consisted of place (n = 11; 23%), head-direction (n = 20; 43%), border (n = 5; 11%) and grid (n = 11;
461 23%) cells. A further 35 (43%) did not show obvious spatial properties, e.g., no clear place field or
462 preferred head direction. Strikingly, no spatial units were recorded in the ATNx animals, although
463 non-spatial units (21), i.e., those showing no preferential firing in specific place or head orientation,
464 were present (Fig. 3B). Electrode tracks are reconstructed in Fig. 1F-H.

465 In order to assess whether this absence of spatial cells in ATNx animals was statistically significant,
466 recordings were selected from Control and ATNx animals that were deemed to be independent, i.e.,
467 performed before and after electrode position was altered (during the habituation period), or were
468 performed several days apart, as electrodes had likely shifted naturally. Recordings were considered

to contain spatial cells or non-spatial cells, regardless of the number of cells recorded or whether the same cell had been recorded previously. The presence of spatial cells and non-spatial cells in the sampled recordings was accumulated in a contingency table (Table 1). The null hypothesis is that the true difference in proportion between the sample estimates is equal to 0. In other words, the percentage of recordings with cells of a certain type is independent of the condition being control or lesion. The results from running a two-sided Barnard's unconditional exact test (Barnard, 1947) for a binomial model on a 2x2 contingency table consisting of the observed frequencies from the Control and ATNx lesion recordings are as follows: for the spatial cells (Control 15/53 vs. ATNx 0/47, Wald statistic 4.574, difference in proportion 0.28, $p < 0.001$), indicating the data strongly supports rejecting the null hypothesis; for the non-spatial cells (Control 16/53 vs. ATNx 13/47, Wald statistic 0.28, difference in proportion 0.0259, $p = 0.81$), indicating that the null hypothesis should not be rejected.

A Bayesian analysis was then conducted on the contingency table data (MacKay and Mac Kay, 2003). We find that (at about 99.99% chance), it is more likely to record a spatial cell in a Control recording, compared to an ATNx lesion recording, $P(PC > PL) = 0.9999$. Similarly, we find that (at about 93.2% chance), it is five times more likely **to** record a spatial cell in a Control recording compared to an ATNx lesion recording, $P(PC > 5 * PL) = 0.9328$. Overall, we find spatial signalling is lost in the subiculum after ATN lesions.

ATN lesions (NMDA) leave non-spatial subiculum firing properties largely unchanged

Spike properties: The mean spike width of all recorded subicular cells pooled into a single group was greater in ATNx animals than Control (Control 155.26 ± 50.43 µs, ATNx 213.88 ± 53.87 µs; $w = 310$, $p < 0.001$, Mann-Whitney U test). Other spike properties (top section, Table 2) showed no differences between groups, including number of spikes (Control 2694 ± 3250, ATNx 4718 ± 6326; $t_{(22.66)} = -1.39$, $p = 0.179$); spike frequency (Control 2.93 ± 4.31 spikes/s, ATNx 5.42 ± 7.07 spikes/s; $w = 809$, $p = 0.673$, Mann-Whitney U test); amplitude (Control 107 ± 31 µV, ATNx 104 ± 19 µV; $t_{(49.3)} = 0.47$, p =

494 0.642); height (Control l 147 ± 54 µV, ATNx 161 ± 39 µV; $t_{(40.74)}$ = -1.34, p = 0.187). We tested the ISI
495 medians for normality using the Shapiro-Wilk test, which indicated these data are not-normally
496 distributed (Control W=0.530, p<.001 ATNx W=0.691, p<.001). We therefore applied a non-
497 parametric Mann Whitney U-test to compare the ISI medians in the Control and ATNx groups. The
498 means of the median ISIs in the Control and ATNx groups were 153 and 547 ms, respectively (Mann–
499 Whitney W=386, p=0.010, two-tailed).

500 When non-spatial cells in Control animals were compared to putative 'non-spatial' cells in ATNx
501 animals, spike width (Control 173 ± 60 µs, ATNx 213 ± 54 µs; $t_{(45.60)}$ = -2.56, p = 0.014, Fig. 4K), and
502 spike height (Control 133 ± 40 µV, ATNx 161 ± 39 µV; $t_{(42.11)}$ = -2.57, p = 0.014, Fig. 4J) were both
503 smaller in Control animals. Spike width was assessed further using histograms to determine whether
504 the difference observed between Control and ATNx reflected different neuron populations (Fig. 5).
505 More short duration waveforms were recorded in Control animals than ATNx, but the samples
506 obtained from the two groups were not distinct (Fig. 5A). Cells with narrow spike widths were more
507 often spatial, but the classification of narrow and wide waveform cells was mixed in both Control
508 and ATNx combined (Fig. 5B) and Control only (Fig. 5C). The mean width for controls of non-spatial
509 cells was 170.6 ± 61.3 µs, while for spatial cells the mean was 142.5 ± 37.5 µs, a significant difference
510 (Mann-Whitney U test, W=962, p = 0.026).

511 *Spike properties of bursting cells:* As no spatial units were recorded in ATNx animals, it was unclear
512 whether spatial cells were present but inhibited (and, therefore, not recorded) or whether the units
513 that were recorded were latent spatial units that were now not responding to 'spatial' inputs. Due to
514 the difficulties in comparing non-spatial units in the Control to unknown spatial or non-spatial units
515 in ATNx animals, subicular cells were classified according to their spike properties into bursting, fast
516 spiking, and theta-entrained cells (Anderson and O'Mara, 2003). While the percentage of subiculum
517 bursting cells in the Control (53% of 82 units) and ATNx (57% of 21) animals was essentially
518 equivalent, other properties differed (lower section Table 2, Fig. 4). Cells in Control animals showed

519 a greater propensity to burst than those in lesion animals (Control 0.12 ± 0.09, ATNx 0.06 ± 0.03;
520 $t_{(35.46)}$ = 3.69, p < 0.001; Table 2). Bursting cells in Control animals showed more spikes per burst
521 (Control 2.13 ± 0.11, ATNx 2.05 ± 0.05; w = 1005, p = 0.004, Mann-Whitney U test) and greater burst
522 duration (Control 5.61 ± 0.64 ms, ATNx 5.07 ± 0.45 ms; $t_{(18.21)}$ = 3.04, p = 0.007), and conversely lesion
523 animals showed larger inter-burst intervals than controls (Control 11144 ± 11074 ms, ATNx 31831 ±
524 39509 ms; $t_{(9.32)}$ = -1.56, p = 0.038; Table 2).

525 **Muscimol infusion reversibly reduces spatial alternation memory performance to chance**

526 When the ATN was temporarily inactivated with muscimol, spatial alternation percentage dropped
527 to chance levels (before muscimol infusion 87.27 ± 7.41; after muscimol infusion 50.00 ± 13.97; Fig.
528 6B). Two animals also received bilateral saline infusions as a control, showing no deficit in spatial
529 alternation (87.5 ± 0%). The muscimol inactivation caused a significant deficit in spatial alternation
530 compared to both before muscimol and saline infusion (ANOVA, $F_{(3, 62)}$ = 49.69, p < 0.001, Tukey
531 *post-hoc* p < 0.001).

532 **Muscimol infusion reversibly abrogates subiculum spatial firing**

533 Prior to the muscimol infusion sessions, electrophysiological recordings were conducted on
534 cannulated rats to allow for electrode adjustment and habituation to recording equipment. Single
535 units were recorded during these habituation periods, however, only units recorded during the
536 inactivation experiments were considered. Thirty-five cells were recorded during muscimol
537 experiments. Of these, 29 were recorded at baseline, i.e., immediately prior to muscimol infusion,
538 and so included in the study (Fig. 6 A1-A3; C1-C3). Of the 29 recorded at baseline, only one cell was
539 recorded prior to infusion and not afterwards.

540 **Muscimol infusion leaves non-spatial subiculum firing properties largely unchanged**

541 *Spike properties:* For analysis, unless otherwise stated, Welch's Two Sample *t*-tests were performed
542 to consider cell parameters with respect to baseline data, with Bonferroni post-hoc correction to

account for multiple comparisons of time points to baseline. When all cells were grouped together, there was no significant change in mean spiking frequency following ATN inactivation (baseline 5.07 ± 9.10 spikes/s, 40-60 min post infusion 2.90 ± 3.84 spikes/s; $t_{(45.21)} = 0.21$, $p = 0.230$), or the number of spikes per recording (baseline 5306 ± 10344, 40-60 min post-infusion 3483 ± 4607; $t_{(46.48)} = 0.89$, $p = 0.378$). Mean spike width (baseline 180.32 ± 55.20 µs, 40-60 min post-infusion 185.81 ± 50.71 µs; $t_{(55.53)} = 0.39$, $p = 0.698$) and amplitude (baseline 113.01 ± 41.43 µV, 40-60 min post-infusion 115.22 ± 45.48 µV; $t_{(51.13)} = 0.19$, $p = 0.851$) showed no change following ATN inactivation when all cells were grouped. A histogram of spike widths showed that while cells with narrow waveforms were more often spatial, the spatial and non-spatial groups remained mixed (Fig. 5D). Finally, when all units were grouped, temporary ATN inactivation led to an apparent doubling of the inter-spike interval (ISI; baseline 664.56 ± 736.57 ms, 40-60 min post-infusion 1443.29 ± 1825.34 ms) although this was not significant ($w = 351$, $p = 0.239$, Mann-Whitney U test).

Following muscimol infusion, spatial properties of subiculum cells declined, despite no decrease in firing frequency. For designated place cells prior to infusion, the place field became disrupted after ATN inactivation (Fig. 6A1). Head directionality also became disrupted without ATN input (Fig. 6A2) and grid cells did not fire in a grid-like pattern (Fig. 6A3). In most cases, these spatial properties were recovered by the following day, although in some cases the cells could no longer be recorded (Fig. 6C3). Interestingly, the subiculum grid cells appeared to lose their place field initially but retained some head directionality, before this too was disrupted (Fig. 6A3, C1-2). We performed an additional control measure by spatially down-sampling the firing maps before and after muscimol injection to match occupancy in each spatial bin.

Spike properties of subiculum bursting cells: Of the 29 units included in the study, at baseline 20 were classified as bursting, 6 fast spiking, and 2 theta modulated (prior to muscimol infusion). For spike property analysis, theta modulated units were excluded due to their high firing frequency and insufficient numbers to perform further statistical analysis. When fast spiking and bursting units

were combined, there was no difference in firing frequency compared to baseline, following ATN inactivation with muscimol (5.07 ± 9.10 spikes/s, 0-20 min post infusion 3.20 ± 4.75 spikes/s; $t_{(52.31)}$ = 0.87, p = 0.385; Fig. 7A). All animals travelled less distance, i.e., showed less activity, as time increased across the experiment (baseline 115.97 ± 33.12 m; 60 - 80 mins 58.17 ± 37.41 m; Fig. 7B), although there was no correlation between firing frequency and distance travelled (r^2 = 0.011; Fig. 7C). Figure 7D illustrates the firing frequency of each cell at baseline, then its frequency in 5 min intervals following muscimol infusion and again the following day, in those instances where the cell was recorded again.

Bursting units did not show any changes in burst properties following inactivation of the ATN, including number of bursts, spikes per burst, and burst duration (p > 0.05). Cells that had been designated as spatial units prior to infusion showed no changes in burst properties or firing frequency, indicating that these spatial cells continue to fire following ATN inactivation but no longer displayed spatial properties.

Anterior thalamic lesions (NMDA) do not affect CA1 place cells, but reduce spatial alternation performance to chance

To explore the effects of anterior thalamic lesions on spatial processing in the dorsal hippocampus, a further three rats were implanted with a microdrive apparatus with 8 recording tetrodes into the dorsal CA1 and received bilateral, permanent (NMDA) lesions of the anterior thalamic nuclei (ATNx_CA1). As in the previous experiment, ATNx_CA1 lesions were quantified by comparing anti-NeuN reacted cell counts in the anterior thalamic nuclei with those from Control. In all ATNx_CA1 animals, the surgery consistently produced a marked cell loss throughout almost the entire anterior thalamic nuclei. An independent sample *t*-test showed significant difference in anti-NeuN cell counts between ATNx_CA1 (4166 ± 1003) and Control (16209 ± 2507; $t_{(7)}$ = 9.08, p < 0.001) groups.

Spatial alternation deficits: As expected, ATNx_CA1 rats showed a deficit in spatial alternation on the T-maze, equivalent to ATNx animals (Control 82.38 ± 11.18, ATNx_CA1 52.60 ± 11.40, $t_{(40.93)}$ = -10.71,

593 $p < 0.001$; Fig. 8C), confirming an impairment in spatial working memory. These animals also showed
594 no deficit in object recognition and no difference in overall exploration time, compared to Control (p
595 > 0.05; Fig. 8D1-3).

596 **CA1 place cells are unaffected by ATN lesions**

597 Daily recordings were conducted in CA1 of ATNx animals (ATNx_CA1) performing a pellet-chasing
598 task in an arena. From these animals, 203 well-isolated units were recorded from dorsal CA1. Units
599 were further classified into 107 spatial units using sparsity and coherence criteria (Schoenenberger
600 et al., 2016) (rat 1 n = 12; rat 2 n = 67; rat 3 n = 28). Putative interneurons were considered to have
601 been recorded from dorsal CA1 if they were recorded on the same tetrode and in the same
602 recording session as a spatial unit. Despite the absence of spatial signals in the subiculum,
603 hippocampal (CA1) place cells appeared intact (Fig. 8E).

604 ## Discussion

605 The origins of diencephalic amnesia remain something of a mystery, despite being described over a
606 century ago (Arts et al., 2017), starkly contrasting with hippocampal amnesia, which has been
607 investigated in breadth and depth since the 1950's (Scoville and Milner, 1957). Clinically,
608 diencephalic amnesia presents as a dense anterograde amnesic syndrome, paralleling the amnesia
609 associated with bilateral hippocampal damage (Arts et al., 2017); the anterior thalamic nuclei appear
610 to be critical structures (Harding et al., 2000; Kril and Harper, 2012). Here, we based our rationale on
611 how the anterior thalamic nuclei project to the hippocampal formation (specifically, the subiculum),
612 but not the hippocampus proper (which includes area CA1). After ATN lesions, CA1 place cell activity
613 appeared preserved, whereas the usual heterogeneous subicular spatial activity (place, head-
614 direction, grid, and border cells) was striking by its absence. Moreover, after ATN lesions,
615 performance fell to chance on a spatial memory task, but remained intact on a non-hippocampal
616 object recognition memory task (Albasser et al., 2012), indicating a specific, rather than generalised,

deficit. The same disruptive effects (behavioural; cellular firing) proved reversible when using transient inactivation (muscimol) of the ATN. Thus, we conclude a key contributor to diencephalic amnesia stems from the loss of anterior thalamic influence on the output regions of the hippocampal formation (Nelson et al., 2020), and, specifically, on the subiculum.

The behavioural effects of our ATN lesions corresponded to those of hippocampal lesions: severely impaired T-maze alternation, but spared object recognition memory in the bow-tie maze (Albasser et al., 2010). ATNx rats showed increased motor activity in square arenas, matching prior evidence of activity increases following ATN lesions in spatial settings (Warburton and Aggleton, 1999; Poirier and Aggleton, 2009; Dumont and Aggleton, 2013). Our extensive ATN lesions largely left CA1 place cells intact (note, there are some reports of microstructural changes and alterations in neuronal activity in CA1 following ATN disruption; Calton et al., 2003; Dillingham et al., 2019). Notably, the proportions of CA1 place cells in ATNx_CA1 animals is in line with our previous experiences of normal animals (Wang et al., 2012; Hok et al., 2012), and that of others (Thompson and Best, 1989; Meshulam et al., 2017; Duvelle et al., 2019; Broussard et al., 2020), contrasting with the more disruptive effects of medial entorhinal cortex lesions on CA1 place cell activity (Hales et al., 2014). As the majority of pyramidal cells in CA1 are place cells, and CA1 heavily innervates the subiculum, it could be assumed that subiculum spatial cells are principally driven by their CA1 inputs, especially as this projection shows activity-dependent plasticity (Commins et al., 1998a,b). The present study revealed, however, CA1 projections alone do not support subicular spatial firing or spatial alternation memory. Rather, anterior thalamic nuclei projections (presumably direct and indirect) are crucial for subicular spatial cellular discharge, and for spatial alternation memory.

The anteroventral nucleus possesses theta-modulated head-direction cells (Tsanov et al., 2011), and the anteromedial nucleus contains place cells and perimeter/boundary cells (Jankowski et al., 2014; Matulewicz et al., 2019). Consistent with previous reports (Sharp and Green, 1994; Brotons-Mas et al., 2010, 2017), we found spatial cells (including grid-like cells), in the dorsal subiculum of control

642 animals. Although grid cells have been widely studied in the hippocampal formation since their
643 discovery (Hafting et al., 2005), the presence of grid cells in the dorsal subiculum is still a relatively
644 new finding (Brotons-Mas et al., 2017). Grid cells have been reported in the presubiculum and
645 parasubiculum (Boccara et al., 2010); both parahippocampal areas receiving anterior thalamic inputs
646 (van Groen and Wyss, 1990). Anterior thalamic lesions disrupt grid cell (and head-direction) activity
647 in these same parahippocampal areas (Goodridge and Taube, 1997; Winter et al., 2015). The grid-
648 like signal found in presubiculum and subiculum might have thalamic (Goodridge and Taube, 1997),
649 and entorhinal (Hafting et al., 2005), components.

650 Stewart and Wong (Stewart and Wong, 1993) originally observed *in vitro* that subicular cells can be
651 classified into bursting and non-bursting classes (confirmed by Sharp and Green, 1994, *in vivo).* A
652 fuller *in vivo* analysis subsequently concluded subicular units could be classified into bursting, regular
653 spiking, theta-modulated, and fast spiking units (Anderson and O'Mara, 2003). Sparsely-bursting
654 subicular cells potentially carry more spatial information (Simonnet and Brecht, 2019). Here,
655 although the proportion of bursting cells in Control and ATNx groups remained equivalent, some
656 properties differed: controls showed a greater burst propensity, more spikes per burst, and greater
657 burst duration. Conversely, lesioned animals showed somewhat larger inter-burst intervals than
658 controls. This alteration in bursting may affect the fidelity of subicular-retrosplenial transmission, as
659 bursting cells in dorsal subiculum with direct connections to granular RSC directly impact sharp-wave
660 ripples in RSC (Nitzan et al., 2020).

661 Given the routes of ATN fibers reaching the medial temporal lobe, it is worth considering if we have
662 recorded from fibers of passage. *In vitro*, "direct recording of single AP (action potential)
663 transmission is challenging" due to the small diameters of axons and recording instability
664 (Radivojevic et al., 2017). However, Robbins et al. (2013) report, in performing hippocampal and
665 alvear recordings, the presence of short-duration triphasic waveforms having a peak-trough length
666 of less than 179 µs, recorded mostly on only one wire of a tetrode. While we recorded for long

667 durations in freely-behaving, implanted animals; our units have a half-width of ~0.8-1.2 ms, within
668 the refractory period for action potentials. Thus, on occasion, we may have recorded from such
669 fibers (e.g., Fig 3A, upper grid cell; but compare Brotons-Mas et al., 2017, Figs 3B and 4C). The
670 possibility of recordings of fibers of passage in subiculum needs further investigation. A different
671 concern relates to the disruption of thalamic fibers of passage. Here, muscimol helped to confirm
672 the NMDA lesions targeted ATN neurons and not fibers of passage (Winter et al., 2015).

673 The subiculum is the primary hippocampal output of area CA1 (Amaral et al., 1991; O'Mara et al.,
674 2001, 2009; Cembrowski et al., 2018), an area with substantial numbers of place cells, suggesting
675 CA1-subiculum inputs are principally spatial. Our data cast new light on this relationship, as CA1
676 inputs are not sufficient to ensure subicular spatial firing. One possibility is the ATN normally exert a
677 direct modulatory, including oscillatory (Vertes et al., 2001), influence on the subiculum that, when
678 removed, leads to changes in gain control, disrupting information processing. Given the range of
679 spatial cells in the ATN (Taube, 1995; Jankowski et al., 2015; Matulewicz et al., 2019), such an input
680 might, for example, help hippocampal and parahippocampal regions co-register their various spatial
681 signals, including those from CA1. This might explain why ATN lesions increased dorsal subiculum
682 spike width and reduced bursting properties, but left other features seemingly intact, e.g., overall
683 spike frequency and amplitude. The latter findings help explain why immediate-early gene analyses
684 have found that ATN lesions can cause hypoactivity in parahippocampal fields, but little apparent
685 impact on the dorsal subiculum (Dillingham et al., 2019).

686 The present findings invoke a wider network account of ATN loss that includes direct efferent
687 actions on the subiculum, alongside indirect actions via parahippocampal and retrosplenial targets.
688 There remains, however, the intriguing issue of why other areas (e.g., CA1, entorhinal cortex, and
689 their outputs) are insufficiently independent of the ATN to preserve subicular spatial firing and
690 ensure effective spatial alternation memory. One clue is the subiculum sends very dense direct and
691 indirect projections to the ATN, i.e., it is a key part of a complex, reciprocal, set of pathways (Bubb et

692 al., 2017). Furthermore, direct anterior thalamic-hippocampal interactions are needed for spatial
693 alternation, irrespective of whether they are ATN projections to the dorsal hippocampus (including
694 subiculum, as examined in the present study), or dorsal subicular projections to the ATN (Nelson et
695 al., 2020). Understanding this reciprocal relationship will prove integral to understanding why ATN
696 damage is such a critical component of diencephalic amnesia (Aggleton and Brown, 1999).

697 The present results demonstrate the critical roles for the ATN in navigation and spatial learning, and
698 spotlight the pivotal role of the subiculum, given the severity of the spatial memory/alternation
699 deficit and the concurrent sparing of CA1 place cells. As the subiculum is a principal source of
700 hippocampal projections beyond the temporal lobe, these findings reveal how anterior thalamic
701 damage might indirectly affect sites such as the mammillary bodies, ventral striatum, and medial and
702 orbital prefrontal cortices (Aggleton et al., 2015; Ferguson et al., 2019; Haugland et al., 2019). These
703 data also indicate signalling within the hippocampus (e.g., CA1) is not sufficient to support the varied
704 spatial signals found in the subiculum. Subicular spatial signals might arise from converging inputs
705 from CA1, the ATN, and parahippocampal areas, including entorhinal cortex. Further work should
706 determine the computations performed by the subiculum on the inputs it receives from ATN to
707 support spatial alternation performance; and to discover how the substantial input from
708 hippocampal area CA1 is gated by ATN inputs reaching the subiculum. Similar considerations suggest
709 a complex origin for diencephalic amnesia, which partly arises from the direct and indirect loss of
710 ATN inputs to output regions of the hippocampal formation. (1496 words)

711 ## References

712 Aggleton JP, Brown MW (1999) Episodic memory, amnesia, and the hippocampal-anterior thalamic
713 axis. Behav Brain Sci 22:425–489.

714 Aggleton JP, Morris RGM (2018) Memory: Looking back and looking forward. Brain Neurosci Adv
715 2:2398212818794830.

716 Aggleton JP, Wright NF, Rosene DL, Saunders RC (2015) Complementary patterns of direct amygdala
717 and hippocampal projections to the macaque prefrontal cortex. Cereb Cortex 25:4351–4373.

718 Albasser MM, Amin E, Lin T-CE, Iordanova MD, Aggleton JP (2012) Evidence that the rat
719 hippocampus has contrasting roles in object recognition memory and object recency memory.
720 Behav Neurosci 126:659.

721 Albasser MM, Chapman RJ, Amin E, Iordanova MD, Vann SD, Aggleton JP (2010) New behavioral
722 protocols to extend our knowledge of rodent object recognition memory. Learn Mem 17:407–
723 419.

724 Amaral DG, Dolorfo C, Alvarez-Royo P (1991) Organization of CA1 projections to the subiculum: a
725 PHA-L analysis in the rat. Hippocampus 1:415–435.

726 Anderson MI, O'Mara SM (2003) Analysis of recordings of single-unit firing and population activity in
727 the dorsal subiculum of unrestrained, freely moving rats. J Neurophysiol 90:655–665.

728 Arts NJM, Walvoort SJW, Kessels RPC (2017) Korsakoff's syndrome: A critical review. Neuropsychiatr
729 Dis Treat.

730 Barnard GA (1947) Significance test for 2x2 tables. Biometrika 34:123–138.

731 Boccara CN, Nardin M, Stella F, O'Neill J, Csicsvari J (2019) The entorhinal cognitive map is attracted
732 to goals. Science 363:1443–1447.

733 Boccara CN, Sargolini F, Thoresen VH, Solstad T, Witter MP, Moser EI, Moser M-B (2010) Grid cells in
734 pre- and parasubiculum. Nat Neurosci 13:987–994.

735 Brotons-Mas JR, Montejo N, O'Mara SM, Sanchez-Vives M V. (2010) Stability of subicular place fields
736 across multiple light and dark transitions. Eur J Neurosci 32:648–658.

737 Brotons-Mas JR, Schaffelhofer S, Guger C, O'Mara SM, Sanchez-Vives M V. (2017) Heterogeneous
738 spatial representation by different subpopulations of neurons in the subiculum. Neuroscience

343:174–189.

Broussard JI, Redell JB, Zhao J, Maynard ME, Kobori N, Perez A, Hood KN, Zhang XO, Moore AN, Dash PK (2020) Mild traumatic brain injury decreases spatial information content and reduces place field stability of hippocampal CA1 neurons. J Neurotrauma 37:227–235.

Bubb EJ, Kinnavane L, Aggleton JP (2017) Hippocampal - diencephalic - cingulate networks for memory and emotion: An anatomical guide. Brain Neurosci Adv 1.

Calton JL, Stackman RW, Goodridge JP, Archey WB, Dudchenko PA, Taube JS (2003) Hippocampal place cell instability after lesions of the head direction cell network. J Neurosci 23:9719–9731.

Cembrowski MS, Phillips MG, DiLisio SF, Shields BC, Winnubst J, Chandrashekar J, Bas E, Spruston N (2018) Dissociable Structural and Functional Hippocampal Outputs via Distinct Subiculum Cell Classes. Cell 173:1280-1292.e18.

Colgin LL (2020) Five Decades of Hippocampal Place Cells and EEG Rhythms in Behaving Rats. J Neurosci 40:54 LP – 60.

Commins S, Gigg J, Anderson M, O'Mara SM (1998a) The projection from hippocampal area CA1 to the subiculum sustains long-term potentiation. Neuroreport 9:847–850.

Commins S, Gigg J, Anderson M, O'Mara SM (1998b) Interaction between paired-pulse facilitation and long-term potentiation in the projection from hippocampal area CA1 to the subiculum. Neuroreport 9:4109–4113.

Commins S, O'Mara SM (2000) Interactions between paired-pulse facilitation, low-frequency stimulation, and behavioral stress in the pathway from hippocampal area CA1 to the subiculum: dissociation of baseline synaptic transmission from paired-pulse facilitation and depression of the. Psychobiology 28:1–11.

Dillingham CM, Milczarek MM, Perry JC, Frost BE, Parker GD, Assaf Y, Sengpiel F, O'Mara SM, Vann

762 SD (2019) Mammillothalamic Disconnection Alters Hippocampocortical Oscillatory Activity and
763 Microstructure: Implications for Diencephalic Amnesia. J Neurosci 39:6696–6713.

764 Dillingham CM, Vann SD (2019) Why Isn't the Head Direction System Necessary for Direction?
765 Lessons From the Lateral Mammillary Nuclei. Front Neural Circuits 13:60.

766 Dumont JR, Aggleton JP (2013) Dissociation of recognition and recency memory judgments after
767 anterior thalamic nuclei lesions in rats. Behav Neurosci 127:415–431.

768 Duvelle É, Grieves RM, Hok V, Poucet B, Arleo A, Jeffery KJ, Save E (2019) Insensitivity of place cells
769 to the value of spatial goals in a two-choice flexible navigation task. J Neurosci 39:2522–2541.

770 Ferguson MA, Lim C, Cooke D, Darby RR, Wu O, Rost NS, Corbetta M, Grafman J, Fox MD (2019) A
771 human memory circuit derived from brain lesions causing amnesia. Nat Commun 10:3497.

772 Goodridge JP, Taube JS (1997) Interaction between the postsubiculum and anterior thalamus in the
773 generation of head direction cell activity. J Neurosci 17:9315–9330.

774 Griffin AL (2015) Role of the thalamic nucleus reunions in mediating interactions between the
775 hippocampus and medial prefrontal cortex during spatial working memory. Front Syst Neurosci
776 9:1–8.

777 Hafting T, Fyhn M, Molden S, Moser M-B, Moser EI (2005) Microstructure of a spatial map in the
778 entorhinal cortex. Nature 436:801–806.

779 Hales JB, Schlesiger MI, Leutgeb JK, Squire LR, Leutgeb S, Clark RE (2014) Medial entorhinal cortex
780 lesions only partially disrupt hippocampal place cells and hippocampus-dependent place
781 memory. Cell Rep 9:893–901.

782 Haugland KG, Sugar J, Witter MP (2019) Development and topographical organization of projections
783 from the hippocampus and parahippocampus to the retrosplenial cortex. Eur J Neurosci
784 50:1799–1819.

785 Hok V, Chah E, Reilly RB, O'Mara SM (2012) Hippocampal dynamics predict interindividual cognitive
786 differences in rats. J Neurosci 32:3540–3551.

787 Irle E, Markowitsch HJ (1982) Widespread cortical projections of the hippocampal formation in the
788 cat. Neuroscience 7:2637–2647.

789 Islam MN, Martin SK, Aggleton JP, O'Mara SM (2019) NeuroChaT: A toolbox to analyse the dynamics
790 of neuronal encoding in freely-behaving rodents in vivo. Wellcome Open Res 4:196.

791 Jankowski MM, Islam MN, Wright NF, Vann SD, Erichsen JT, Aggleton JP, O'Mara SM (2014) Nucleus
792 reuniens of the thalamus contains head direction cells. Elife 3:1–10.

793 Jankowski MM, Passecker J, Islam MN, Vann S, Erichsen JT, Aggleton JP, O'Mara SM (2015) Evidence
794 for spatially-responsive neurons in the rostral thalamus. Front Behav Neurosci 9:256.

795 Jay TM, Witter MP (1991) Distribution of hippocampal CA1 and subicular efferents in the prefrontal
796 cortex of the rat studied by means of anterograde transport of Phaseolus vulgaris-
797 leucoagglutinin. J Comp Neurol 313:574–586.

798 Kril JJ, Harper CG (2012) Neuroanatomy and neuropathology associated with Korsakoff's syndrome.
799 Neuropsychol Rev 22:72–80.

800 MacKay DJC, Mac Kay DJC (2003) Information theory, inference and learning algorithms. Cambridge
801 university press.

802 Matulewicz P, Ulrich K, Islam MN, Mathiasen ML, Aggleton JP, O'Mara SM (2019) Proximal perimeter
803 encoding in the rat rostral thalamus. Sci Rep 9:1–12.

804 Meibach RC, Siegel A (1977) Subicular projections to the posterior cingulate cortex in rats. Exp
805 Neurol 57:264–274.

806 Meshulam L, Gauthier JL, Brody CD, Tank DW, Bialek W (2017) Collective behavior of place and non-
807 place neurons in the hippocampal network. Neuron 96:1178–1191.

808 Moran JP, Dalrymple-Alford JC (2003) Perirhinal cortex and anterior thalamic lesions: comparative
809 effects on learning and memory. Behav Neurosci 117:1326–1341.

810 Morris RG, Garrud P, Rawlins JN, O'Keefe J (1982) Place navigation impaired in rats with
811 hippocampal lesions. Nature 297:681–683.

812 Nelson AJD, Kinnavane L, Amin E, O'Mara SM, Aggleton JP (2020) Deconstructing the direct
813 reciprocal hippocampal-anterior thalamic pathways for spatial learning. J Neurosci 40:6978–
814 6990.

815 Nitzan N, McKenzie S, Beed P, English DF, Oldani S, Tukker JJ, Buzsáki G, Schmitz D (2020)
816 Propagation of hippocampal ripples to the neocortex by way of a subiculum-retrosplenial
817 pathway. Nat Commun 11:1947.

818 O'Mara SM, Aggleton JP (2019) Space and Memory (Far) Beyond the Hippocampus: Many
819 Subcortical Structures Also Support Cognitive Mapping and Mnemonic Processing. Front Neural
820 Circuits 13:1–12.

821 O'Mara SM, Commins S, Anderson M (2000) Synaptic plasticity in the hippocampal area CA1-
822 subiculum projection: Implications for theories of memory. Hippocampus 10.

823 O'Mara SM, Commins S, Anderson M, Gigg J (2001) The subiculum: A review of form, physiology and
824 function. Prog Neurobiol 64.

825 O'Mara SM, Sanchez-Vives MV, Brotons-Mas JR, O'Hare E (2009) Roles for the subiculum in spatial
826 information processing, memory, motivation and the temporal control of behaviour. Prog
827 Neuro-Psychopharmacology Biol Psychiatry 33.

828 Peyrache A, Duszkiewicz AJ, Viejo G, Angeles-Duran S (2019) Thalamocortical processing of the head-
829 direction sense. Prog Neurobiol 183:101693.

830 Poirier GL, Aggleton JP (2009) Post-surgical interval and lesion location within the limbic thalamus

determine extent of retrosplenial cortex immediate-early gene hypoactivity. Neuroscience 160:452–469.

Preibisch S, Saalfeld S, Tomancak P (2009) Globally optimal stitching of tiled 3D microscopic image acquisitions. Bioinformatics 25:1463–1465.

Radivojevic M, Franke F, Altermatt M, Müller J, Hierlemann A, Bakkum DJ (2017) Tracking individual action potentials throughout mammalian axonal arbors. Elife 6:e30198.

Ranganath C, Ritchey M (2012) Two cortical systems for memory-guided behaviour. Nat Rev Neurosci 13:713–726.

Robbins AA, Fox SE, Holmes GL, Scott RC, Barry JM (2013) Short duration waveforms recorded extracellularly from freely moving rats are representative of axonal activity. Front Neural Circuits 7:181.

Schoenenberger P, O'Neill J, Csicsvari J (2016) Activity-dependent plasticity of hippocampal place maps. Nat Commun 7:11824.

Scoville WB, Milner B (1957) Loss of recent memory after bilateral hippocampal lesions. J Neurol Neurosurg Psychiatry 20:11–21.

Sharp PE, Green C (1994) Spatial correlates of firing patterns of single cells in the subiculum of the freely moving rat. J Neurosci 14:2339–2356.

Shibata H (1993) Direct projections from the anterior thalamic nuclei to the retrohippocampal region in the rat. J Comp Neurol 337:431–445.

Simonnet J, Brecht M (2019) Burst firing and spatial coding in subicular principal cells. J Neurosci 39:3651–3662.

Skaggs WE, McNaughton BL, Wilson MA, Barnes CA (1996) Theta phase precession in hippocampal neuronal populations and the compression of temporal sequences. Hippocampus 6:149–172.

854 Spiers HJ, Maguire EA, Burgess N (2001) Hippocampal amnesia. Neurocase 7:357–382.

855 Stewart M, Wong RK (1993) Intrinsic properties and evoked responses of guinea pig subicular
856 neurons in vitro. J Neurophysiol 70:232–245.

857 Sutherland RJ, Rodriguez AJ (1989) The role of the fornix/fimbria and some related subcortical
858 structures in place learning and memory. Behav Brain Res 32:265–277.

859 Taube JS (1995) Head direction cells recorded in the anterior thalamic nuclei of freely moving rats. J
860 Neurosci 15:70–86.

861 Thompson LT, Best PJ (1989) Place cells and silent cells in the hippocampus of freely-behaving rats. J
862 Neurosci 9:2382–2390.

863 Tsanov M, Chah E, Vann SD, Reilly RB, Erichsen JT, Aggleton JP, O'Mara SM (2011) Theta-modulated
864 head direction cells in the rat anterior thalamus. J Neurosci 31:9489–9502.

865 van Groen T, Wyss JM (1990) The connections of presubiculum and parasubiculum in the rat. Brain
866 Res 518:227–243.

867 Vertes RP, Albo Z, Viana Di Prisco G (2001) Theta-rhythmically firing neurons in the anterior
868 thalamus: implications for mnemonic functions of Papez's circuit. Neuroscience 104:619–625.

869 Wang BW, Hok V, Della-Chiesa A, Callaghan C, Barlow S, Tsanov M, Bechara R, Irving E, Virley DJ,
870 Upton N, O'Mara SM (2012) Rosiglitazone enhances learning, place cell activity, and synaptic
871 plasticity in middle-aged rats. Neurobiol Aging 33.

872 Warburton EC, Aggleton JP (1999) Differential deficits in the Morris water maze following cytotoxic
873 lesions of the anterior thalamus and fornix transection. Behav Brain Res 98:27–38.

874 Winter SS, Clark BJ, Taube JS (2015) Spatial navigation. Disruption of the head direction cell network
875 impairs the parahippocampal grid cell signal. Science 347:870–874.

Figure and Table Legends

Figure 1

NeuN-reacted coronal sections showing the status of the anterior thalamic nuclei (ATN) in control (A) and lesion (B) animals. The nucleus reuniens (arrowed), as shown using calbindin-reacted sections, was intact in both control (C) and lesion (D) animals, indicating that reuniens damage was not responsible for deficits seen in ATN lesioned animals. (E) The ATN cell count was significantly reduced in lesioned animals (ATNx) compared to controls (Control). Nissl-stained coronal sections helped to confirm electrode placement in dorsal subiculum (F), with the electrode path indicated. (G) Schematic representing cannula placement (blue) and the two targets of the infusion needle (red). (H) Cresyl violet stained section indicating cannula placement, with DAB-reacted flurogold infused to indicate spread of muscimol, with the black line indicating canula placement and red indicating the track of the infusion needle, and dashed white to indicate the spread of the muscimol. *** = $p < 0.001$ (Welch's Two Sample *t*-test). Scale bar = 800 µm.

Figure 2

(A) Schematic diagram of spatial alternation task. ATN lesioned animals (ATNx) showed a significant deficit in spatial alternation compared to both control and sham animals (B). (C) Schematic of novel object recognition task. There was no difference between control (Control) and lesion rats in cumulative D1 (D), D2 (E), or total exploration time (F). *** $p < 0.001$ (ANOVA with Tukey post-hoc), error bars represent SEM.

Figure 3

Representative single units recorded in the dorsal subiculum in control (Control; A) and ATN lesion (ATNx; B) animals. For individual units the figures illustrate: Heatmap of spike location adjusted for time spent in each location; path in arena (black) with spike location (blue); head direction; mean spike waveform. For the Control group, different classes of spatial cells are displayed, along with a non-spatial cell. No spatial cells were recorded in the ATNx cases. HD, head direction.

Figure 4

Properties of bursting and non-spatial subicular cells. (A, B) Waveforms and autocorrelation histograms were used for cell classification. (C) Diagram of waveform properties. Bursting cells in Control showed a higher burst duration (E), had more spikes per burst (F), and had a higher propensity to burst (H). Bursting cells in ATNx had a greater spike width (D) and higher inter-burst interval (I), than non-bursting cells. (J, K) Non-spatial cells in ATN had higher spike width and spike height than non-spatial cells in Control animals. For boxplots (D-K), filled circles indicate outliers and unfilled diamonds indicate the mean. * $p < 0.05$, ** $p < 0.01$, *** $p < 0.001$ (Welch's Two Sample *t*-test or Mann-Whitney U test).

Figure 5

(A) When Control rats are compared to rats with permanent NMDA lesions of the ATN (ATNx), more short duration waveforms were recorded in Controls, but the samples obtained from the two groups of rats are not distinct. (B, C) In the permanent lesion study, narrow waveform cells were more often spatial, but the classification of wide and narrow waveform cells was mixed. B presents combined data for the Control and ATNx rats, while C

presents data for only Control rats. (D) Similarly, in rats where the ATN was inactivated with muscimol, narrow waveform cells were more often spatial, but the groups were mixed.

Figure 6

(A1-A3) Examples of spatial units before, during and after muscimol infusion. Spatial properties of single units decreased when ATN was inactivated. (Note, unit A3 showed relative inactivity after 100-120 minutes, and the cell was not recorded the next day). (B) Spatial alternation dropped to chance levels when the ATN were temporarily inactivated with muscimol, compared to the same animals prior to infusion. When saline was infused in place of muscimol no deficit was present. (C1-C3) further examples of spatial units before and after ATN inactivation. C1 shows disruption of place field shortly after muscimol infusion with some head directionality remaining, which was later disrupted. For (C3), no firing was detected after muscimol infusion. ** = $p < 0.01$ (ANOVA with Tukey post-hoc).

Figure 7

Spike properties following temporary inactivation of ATN with muscimol (M). (A) Inactivation of ATN caused no significant decrease in single unit firing frequency. (B) Animals showed decreasing levels of activity throughout the experiment, although there was no significant correlation between distance travelled and spike frequency (C). (D) Represents firing frequency of each cell recorded at baseline (left), in 5 minute bins throughout the experiment. The first white line indicates ATN inactivation with muscimol, after 15-20 minutes of baseline recording before infusion. In most cases, electrophysiological recording was paused for T-maze testing between 80-100 minutes (second and third white lines), then continued. Recordings in which the animal was largely inactive or asleep were excluded. The

final white line indicates data from the day after infusion. (E) There were no significant changes in spike firing in spatial units as a result of ATN inactivation and burst properties remained consistent including the number of bursts (F). (A, B, E, F) First red vertical line ('M') indicates the infusion of muscimol, second red vertical line indicates recordings taken the next day ('ND'). Each bin represents 20 minutes of recording. Data are compared to baseline, immediately prior to inactivation, with error bars indicating SEM. Theta entrained cells are removed from A, B and C due to high firing frequency compared to other cell classes. *** $p < 0.001$ (Welch's Two Sample *t*-test with Bonferroni correction).

Figure 8

Representative electrode placement in CA1 (A) and ATN lesion (B), in NeuN-reacted sections. (C) Animals with ATN lesions and electrodes implanted in CA1 showed a significant deficit in spatial alternation task compared to Control animals (control data repeated from experiment 1). (D1-D3) The same cohort of ATNx animals showed no deficit in object recognition on bow tie maze. (E) Representative place cells recorded from CA1 in three ATNx animals.

Table 1

Recordings from Control and ATNx animals (where a 'recording' is defined as a single trial of an open field recording session) were selected such that recordings were independent. Recordings were deemed to be independent if they were performed before and after adjustment of electrode position, or if they were several days apart, as the electrodes had likely shifted naturally. For each of these recordings, the presence or absence of both spatial

cells and non-spatial cells were marked, and the observed frequencies are presented in the table.

Table 2

Summary of spike and burst properties of subicular units. Duty cycle describes the portion of the inter-burst interval during which a burst fires. * $p < 0.05$, ** $p < 0.01$, *** $p < 0.001$ (Welch's Two Sample *t*-test).

Figures and Tables

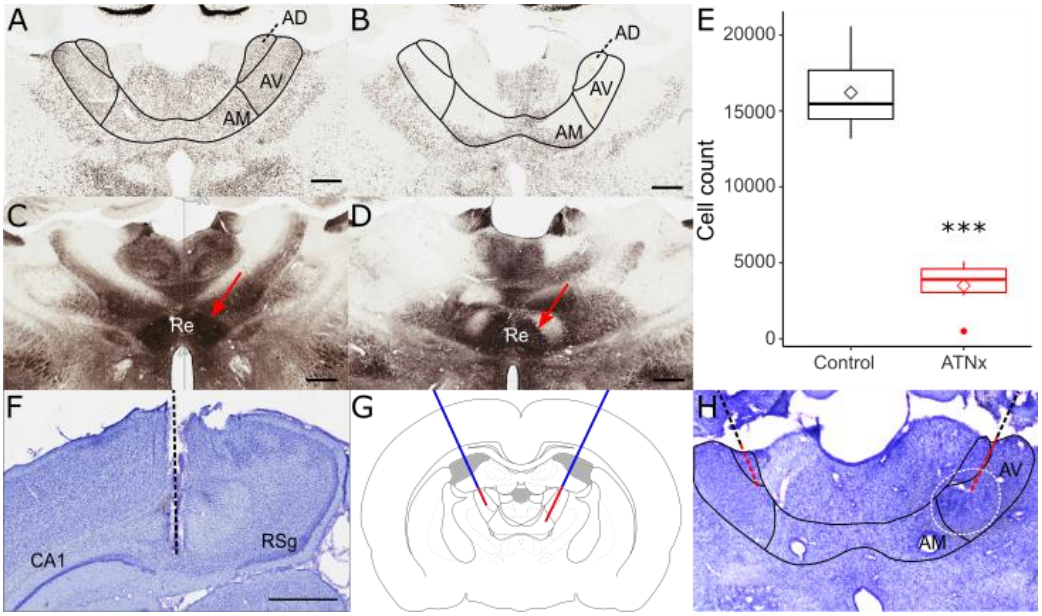

Fig. 1: NeuN-reacted coronal sections showing the status of the anterior thalamic nuclei (ATN) in control (A) and lesion (B) animals. The nucleus reuniens (arrowed), as shown using calbindin-reacted sections, was intact in both control (C) and lesion (D) animals, indicating that reuniens damage was not responsible for deficits seen in ATN lesioned animals. (E) The ATN cell count was significantly reduced in lesioned animals (ATNx) compared to controls (Control). Nissl-stained coronal sections helped to confirm electrode placement in dorsal subiculum (F), with the electrode path indicated. (G) Schematic representing cannula placement (blue) and the two targets of the infusion needle (red). (H) Cresyl violet stained section indicating cannula placement, with

DAB-reacted flurogold infused to indicate spread of muscimol, with the black line indicating canula placement and red indicating the track of the infusion needle, and dashed white to indicate the spread of the muscimol. *** = $p < 0.001$ (Welch's Two Sample *t*-test). Scale bar = 800 µm.

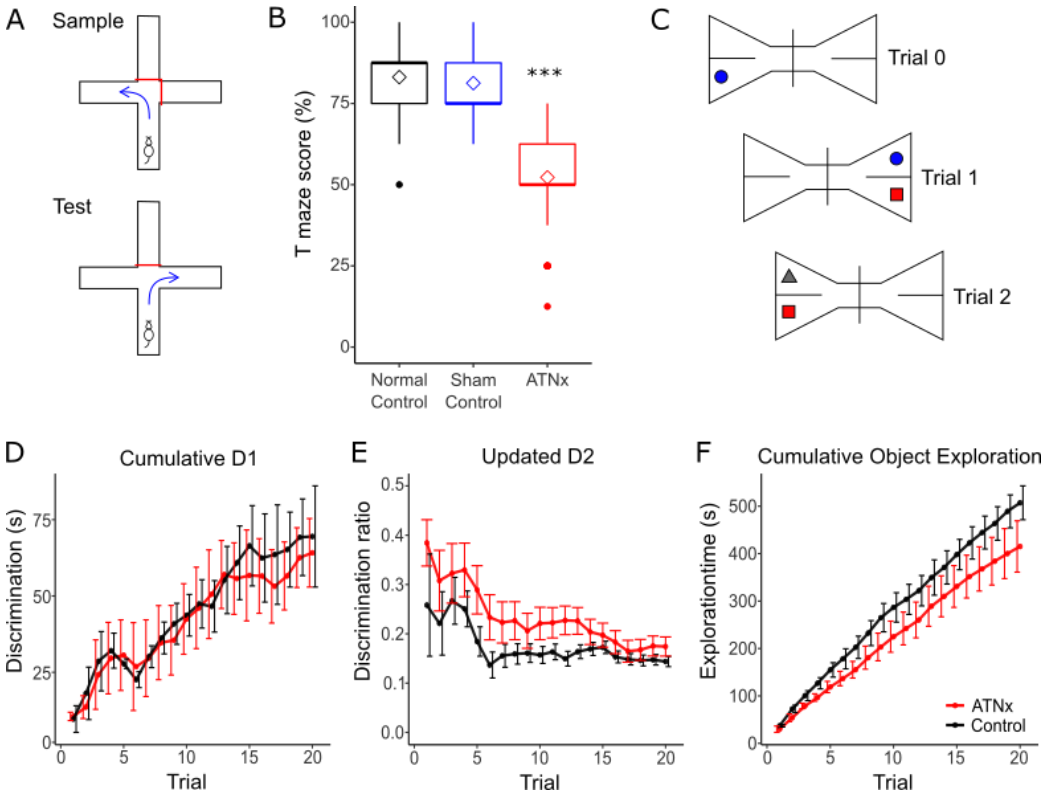

979

980 **Fig. 2:** (A) Schematic diagram of spatial alternation task. ATN lesioned animals (ATNx) showed a significant
981 deficit in spatial alternation compared to both control and sham animals (B). (C) Schematic of novel object
982 recognition task. There was no difference between Control and lesion rats in cumulative D1 (D), D2 (E), or total
983 exploration time (F). *** $p < 0.001$ (ANOVA with Tukey *post-hoc*), error bars represent SEM.

984

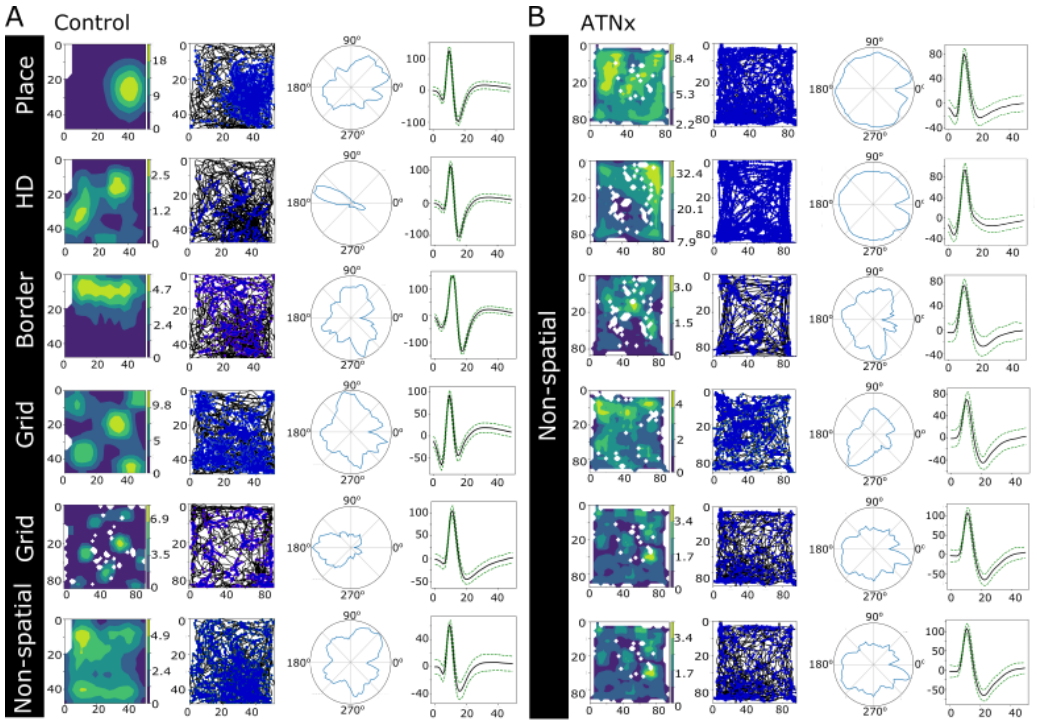

Fig. 3: Representative single units recorded in the dorsal subiculum in control (Control; A) and ATN lesion (ATNx; B) animals. For individual units the figures illustrate: Heatmap of spike location adjusted for time spent in each location; path in arena (black) with spike location (blue); head direction; mean spike waveform. For the Control group, different classes of spatial cells are displayed, along with a non-spatial cell. No spatial cells were recorded in the ATNx cases. HD, head direction.

Observed frequencies for recordings	Control	Lesion	Total
Spatial cells			
At least one spatial cell was recorded	15	0	15
Spatial cells were not recorded	38	47	85
Total recordings performed	53	47	100
Non-Spatial cells			
At least one non-spatial cell was recorded	16	13	29
Non-spatial cells were not recorded	37	34	61
Total recordings performed	53	47	100

992

993 **Table 1:** Recording counts from Control and ATNx animals

994 Recordings from Control and ATNx animals (where a 'recording' is defined as a single trial of an open field
995 recording session) were selected such that recordings were independent. Recordings were deemed to be
996 independent if they were performed before and after adjustment of electrode position, or if they were several
997 days apart, as the electrodes had likely shifted naturally. For each of these recordings, the presence or absence
998 of both spatial cells and non-spatial cells were marked, and the observed frequencies are presented in the
999 table.

1000

	Control		ATNx (Lesion)	
	Mean	**± SD**	**Mean**	**± SD**
Number of spikes (per 20 minutes)	2694.93	3249.93	4718.00	6326.09
Spike rate (spikes/s)	2.93	4.31	5.42	7.07
Spike amplitude (μV)	106.91	31.15	104.33	19.20
Spike height (μV)	146.91	53.96	161.18	39.32
Spike width (μs) ***	155.26	50.43	213.88	53.87
Inter-spike interval (ISI; ms)	1008.59	1381.03	2253.24	3453.02
Total bursts (per 20 minutes)	238.90	435.98	116.6	157.78
Total bursting spikes (per 20 minutes)	526.59	981.86	242.90	331.59
Mean bursting ISI (ms)	4.08	0.32	3.88	0.28
Spikes per burst *	2.13	0.11	2.05	0.05
Mean burst duration (ms) *	5.61	0.64	5.07	0.45
Inter-burst interval (ms) *	11144.49	11073.79	31830.77	39508.75
Mean duty cycle (burst duration / inter-burst interval)	0.05	0.05	0.02	0.02
Propensity to burst (bursting spikes / total spikes) ***	0.12	0.09	0.06	0.03

1001 **Table 2:** Summary of spike and burst properties of subicular units.

1002 Duty cycle describes the portion of the inter-burst interval during which a burst fires. * $p < 0.05$, ** $p < 0.01$,

1003 *** $p < 0.001$ (Welch's Two Sample *t*-test).

1004

1005

1006

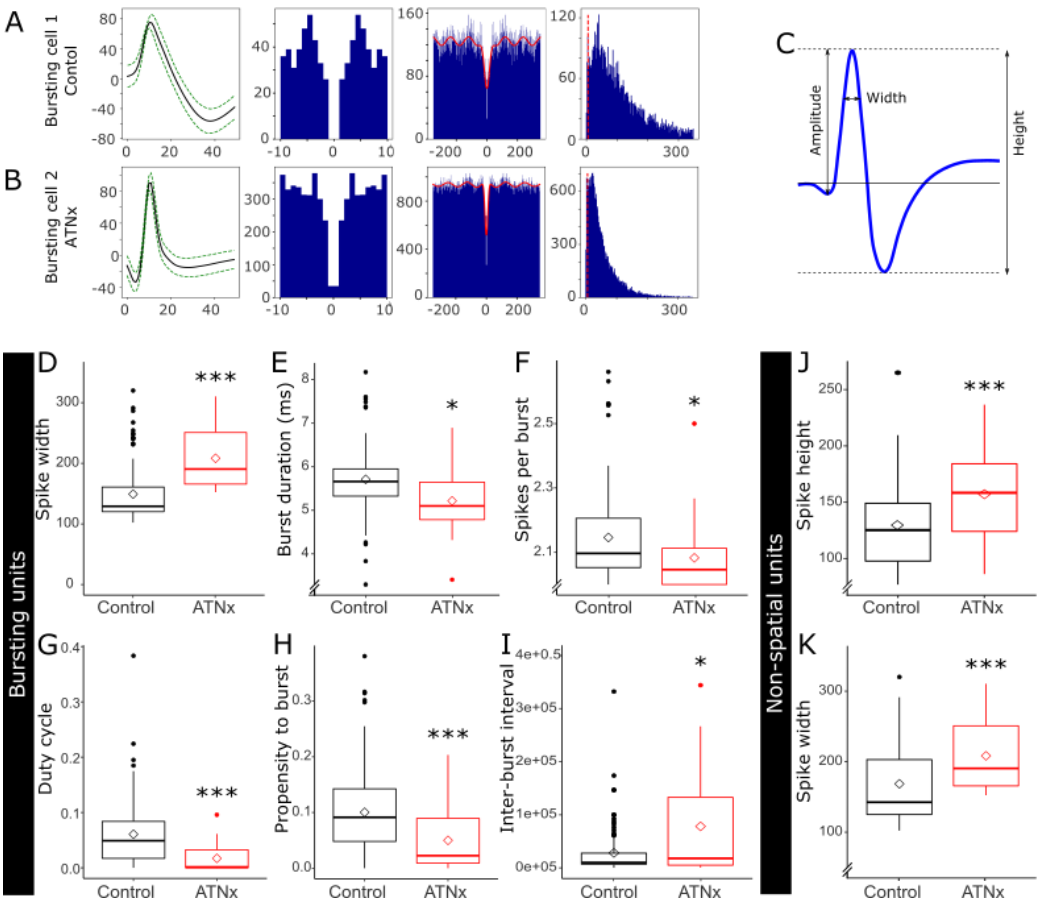

Fig. 4: Properties of bursting and non-spatial subicular cells. (A, B) Waveforms and autocorrelation histograms were used for cell classification. (C) Diagram of waveform properties. Bursting cells in Control showed a higher burst duration (E), had more spikes per burst (F), and had a higher propensity to burst (H). Bursting cells in ATNx had a greater spike width (D) and higher inter-burst interval (I), than non-bursting cells. (J, K) Non-spatial cells in ATN had higher spike width and spike height than non-spatial cells in Control animals. For boxplots (D-K), filled circles indicate outliers and unfilled diamonds indicate the mean. * $p < 0.05$, ** $p < 0.01$, *** $p < 0.001$ (Welch's Two Sample *t*-test or Mann-Whitney U test).

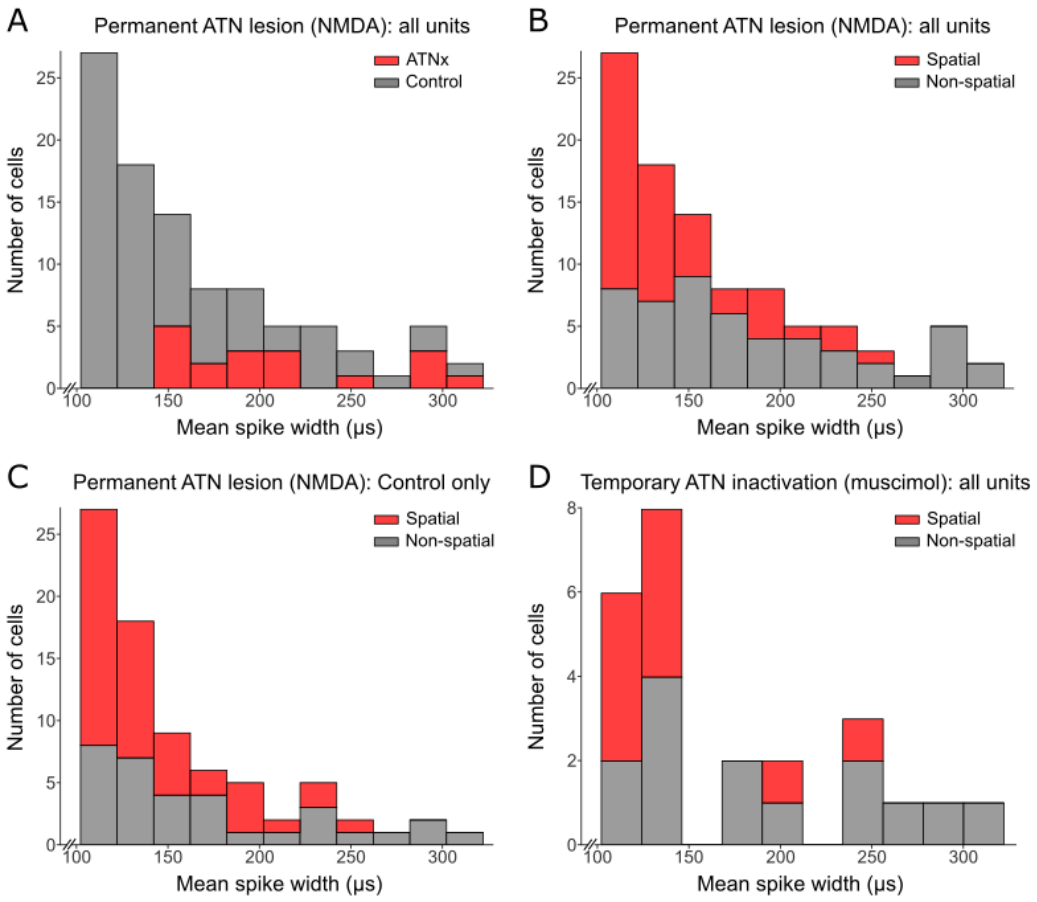

1016

1017 **Fig. 5:** (A) When Control rats are compared to rats with permanent NMDA lesions of the ATN (ATNx), more
1018 short duration waveforms were recorded in Controls, but the samples obtained from the two groups of rats
1019 are not distinct. (B, C) In the permanent lesion study, narrow waveform cells were more often spatial, but the
1020 classification of wide and narrow waveform cells was mixed. B presents combined data for the Control and
1021 ATNx rats, while C presents data for only Control rats. (D) Similarly, in rats where the ATN was inactivated with
1022 muscimol, narrow waveform cells were more often spatial, but the groups were mixed.

1023

1024

1025

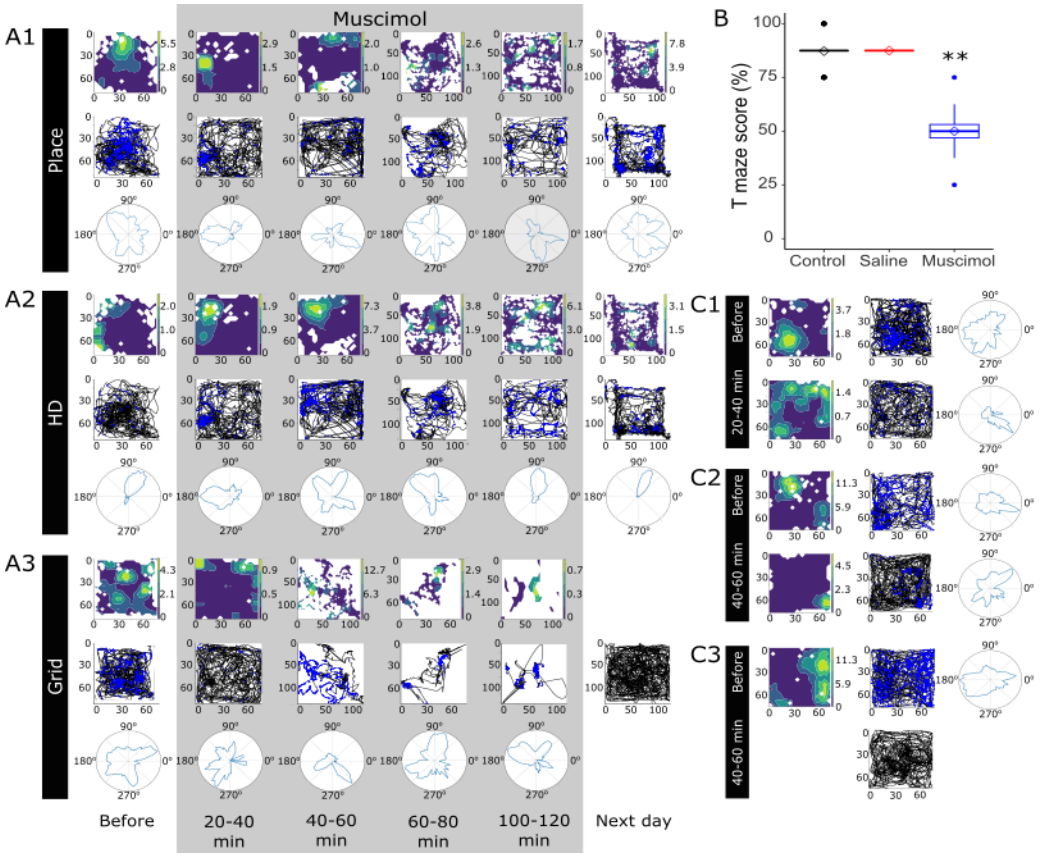

Fig. 6: (A1-A3) Examples of spatial units before, during and after muscimol infusion. Spatial properties of single units decreased when ATN was inactivated. (Note, unit A3 showed relative inactivity after 100-120 minutes, and the cell was not recorded the next day). (B) Spatial alternation dropped to chance levels when the ATN were temporarily inactivated with muscimol, compared to the same animals prior to infusion. When saline was infused in place of muscimol no deficit was present. (C1-C3) further examples of spatial units before and after ATN inactivation. C1 shows disruption of place field shortly after muscimol infusion with some head directionality remaining, which was later disrupted. For (C3), no firing was detected after muscimol infusion. ** = $p < 0.01$ (ANOVA with Tukey *post-hoc*).

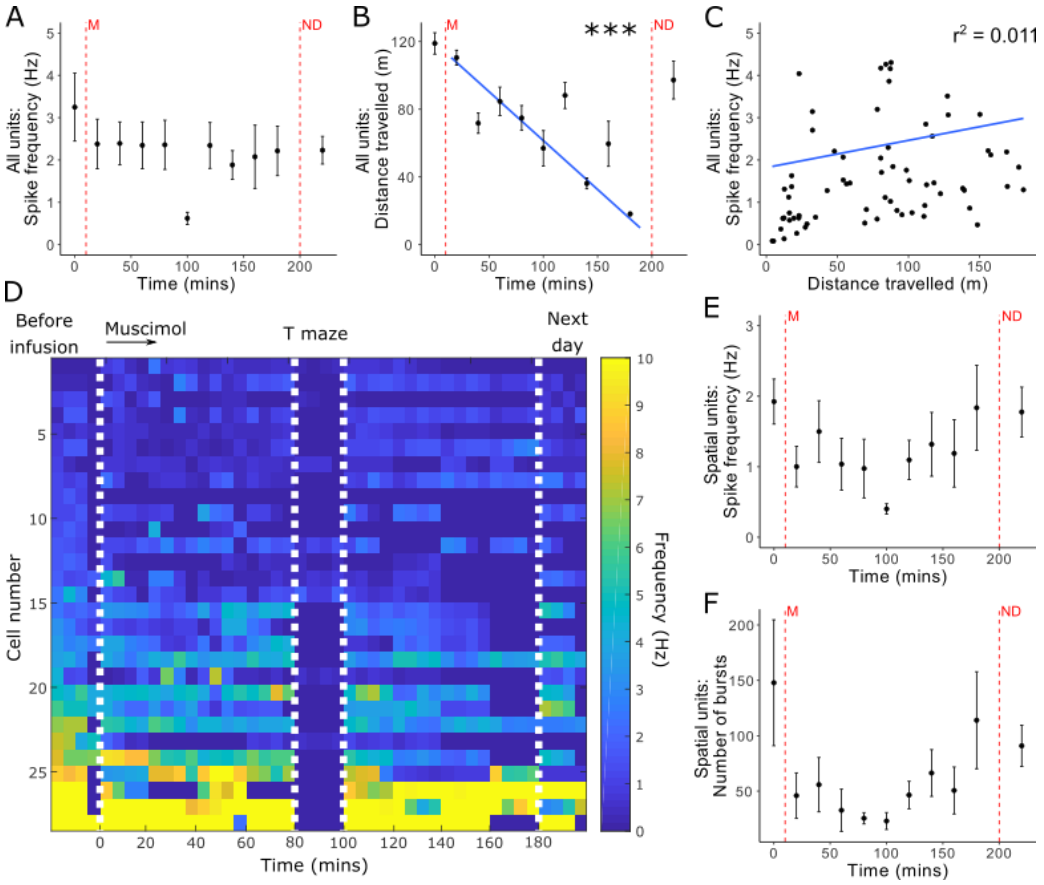

Fig 7: Spike properties following temporary inactivation of ATN with muscimol (M). (A) Inactivation of ATN caused no significant decrease in single unit firing frequency. (B) Animals showed decreasing levels of activity throughout the experiment, although there was no significant correlation between distance travelled and spike frequency (C). (D) Represents firing frequency of each cell recorded at baseline (left), in 5 minute bins throughout the experiment. The first white line indicates ATN inactivation with muscimol, after 15-20 minutes of baseline recording before infusion. In most cases, electrophysiological recording was paused for T-maze between 80-100 minutes (second and third white lines), then continued. Recordings in which the animal was largely inactive or asleep were excluded. The final white line indicates data from the day after infusion. (E) There were no significant changes in spike firing in spatial units because of ATN inactivation and burst properties remained consistent including the number of bursts (F). (A, B, E, F) First red vertical line ('M') indicates the infusion of muscimol, second red vertical line indicates recordings taken the next day ('ND'). Each bin represents 20 minutes of recording. Data are compared to baseline, immediately prior to inactivation, with

1050 error bars indicating SEM. Theta entrained cells are removed from A, B and C due to high firing frequency
1051 compared to other cell classes. *** $p < 0.001$ (Welch's Two Sample *t*-test with Bonferroni correction).

1052

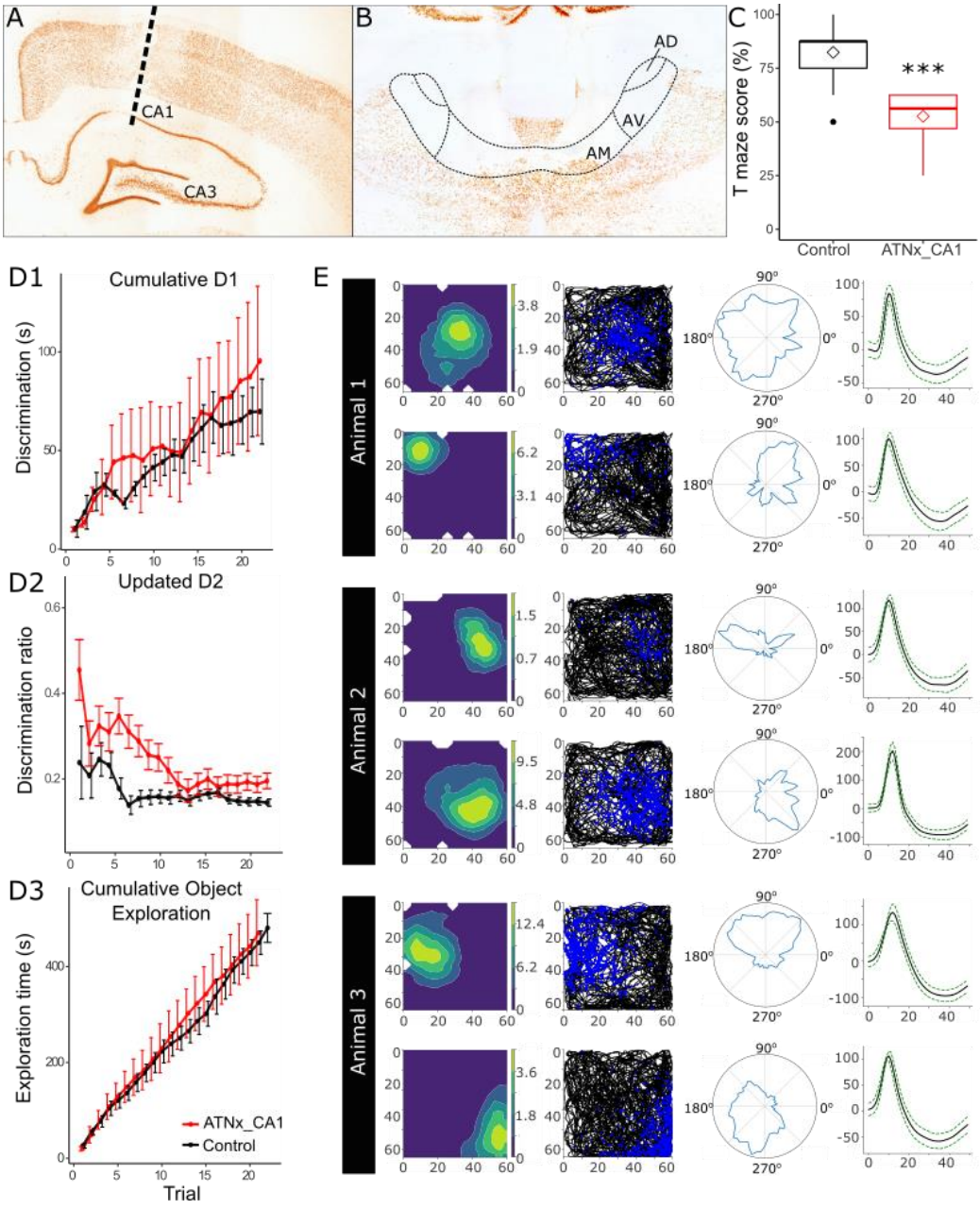

1053

1054 **Fig 8:** Representative electrode placement in CA1 (A) and ATN lesion (B), in NeuN-reacted sections. (C) Animals
1055 with ATN lesions (ATNx) and electrodes implanted in CA1 showed a significant deficit in spatial alternation task
1056 compared to Control animals (control data repeated from experiment 1). (D1-D3) The same cohort of ATNx
1057 animals showed no deficit in object recognition on bow tie maze. (E) Representative place cells recorded from
1058 CA1 in three ATNx animals.